SUPPLEMENTARY METHODS

Materials and Drug Administration. 1-(2,5-dimethoxy-4-iodophenyl)-2-aminopropane (DOI), 1-(2,5-dimethoxy-4-methylphenyl)-2-aminopropane (DOM), 1-(2,5-dimethoxy-4-bromophenyl)-2-aminopropane DOB, lysergic acid diethylamide (LSD), and lisuride hydrogen maleate (lisuride) were purchased from Sigma-Aldrich. (1R,4R,5S,6R)-4-Amino-2-oxabicyclo[3.1.0]hexane-4,6-dicarboxylic acid (LY379268) was obtained from Eli Lilly and Company. 2S-2-amino-2-(1S,2S-2-carboxycyclopropan-1-yl)-3-(xanth-9-yl)-propionic acid (LY341495), (2S,2'R,3'R)-2-(2',3'-dicarboxycyclopropyl)-glycine (DCG-IV), (2S,1'S,2'S)-2-(carboxycyclopropyl)-glycine (L-CCG-I), clozapine, and haloperidol were obtained from Tocris Cookson Inc. [^{3}H]Ketanserin and [^{35}S]GTPγS were purchased from PerkinElmer Life and Analytical Sciences, Inc. [^{3}H]LY341495 was purchased from American Radiolabeled Chemicals, Inc. The injected doses (i.p.) were DOI, 2 mg/kg; DOM, 4 mg/kg; DOB, 1 mg/kg; LSD, 0.24 mg/kg; lisuride, 0.4 mg/kg; ergotamine, 0.5 mg/kg; LY379268, 15 mg/kg; LY341495, 6 mg/kg; clozapine, 25 mg/kg; and haloperidol, 1 mg/kg, unless otherwise indicated.

Transient Transfection of HEK293 cells. HEK293 were maintained in Dulbecco's modified Eagle's medium supplemented with 10% (v/v) foetal bovine serum at 37°C in a 5% CO_2 humidified atmosphere. Transfection was performed using Lipofectamine 2000 reagent (Invitrogen) according to manufacturer's instructions. HEK293 cells stably expressing human 2AR have been described previously[1,2].

Co-immunoprecipitation Studies. Co-immunoprecipitation studies in *postmortem* human brain, and co-immunoprecipitation studies using N-terminally c-myc tagged form of 2AR, and N-terminally haemagglutinin (HA) tagged forms of mGluR2, mGluR3 or mGluR2/mGluR3 chimeras in HEK293 were performed as previously described with minor modifications[3]. Briefly, the samples were incubated overnight with protein A/G beads and anti-2AR (*postmortem* human brain) or anti-c-myc antibody (HEK293 cells) at 4°C on a rotating wheel. Equal amounts of proteins were resolved by SDS-polyacrylamide gel electrophoresis. Detection of proteins by immunoblotting using anti-2AR (Santa Cruz Biotechnology), anti-mGluR2 and anti-mGluR3 (Abcam Inc.) in *postmortem* human brain, or anti-c-myc and anti-HA antibodies (Santa Cruz Biotechnology) in HEK293 was conducted using ECL system according to the manufacturer's recommendations.

Bioluminiscence Resonance Energy Transfer (BRET^2) in HEK293 live cells. The human 2AR, serotonin 5-HT_{2C} (2CR), mGluR2, and mGluR3 receptors with mutated stop codons were subcloned into the p*R*luc and pGFP^2 plasmids (PerkinElmer Life Sciences), such that *Renilla* luciferase (*R*luc) and Green Fluorescent Protein (GFP^2) were present at the C-termini of the receptors. All sequences were confirmed by DNA sequencing. After 48 h, transfected cells were washed with PBS, suspended to 1-2 $\times$ 10^6 cells/ml, and were treated with DeepBlueC Coelenterazine Substrate (5 μM final concentration; PerkinElmer Life Sciences). Equivalents amounts of total DNA comprised of various ratios of the *R*luc- or GFP^2-tagged receptors were transfected[4]. Light emission was monitored

by using a Fusion Universal Microplate Analyzer (PerkinElmer Life Sciences). A BRET^2 signal is defined as the light emitted by GFP^2 at 515 nm in response to the light emitted at 410 nm by *R*luc in upon catalysis of DeepBlueC. The values were corrected by subtracting the background BRET^2 signal detected when the receptor-*R*luc construct was expressed alone (see Supplementary Fig. S3 for luminescence and fluorescence values). The specificity of mGluR2-*R*luc and 2AR-GFP^2 interactions were assessed by comparison with co-expression of mGluR2-*R*luc and 2CR-GFP^2, mGluR3-*R*luc and 2AR-GFP^2 and mGluR2-*R*luc and GFP^2. Data from a single experiment, which has been replicated three times, are displayed as mean±s.e.m. (Fig. 1e).

Fluorescence Resonance Energy Transfer (FRET). Forms of the 2AR and mGluR2 C-terminally fused to eCFP and eYFP were generated, and FRET microscopy in living cells was conducted as previously reported[3]. Results from a single experiment, representative of two-three independent studies, are shown in Fig. 2d.

[^{3}H]Ketanserin, [^{3}H]LY341495 and [^{35}S]GTPγS Binding. Membrane preparations and [^{3}H]ketanserin binding assays were performed as previously reported[5]. [^{3}H]LY341495 binding was performed as previously described with minor modifications[6]. Briefly, membrane preparations were incubated for 60 min at 4°C. Non-specific binding was determined in the presence of 1mM L-glutamate. [^{35}S]GTPγS binding experiments were initiated by the addition of membranes containing 35 μg protein to an assay buffer (20 mM HEPES, 3 mM $MgCl_2$, 100 mM NaCl, 0.2 mM ascorbic acid, and 0.5 nM [^{35}S]GTPγS)

supplemented with 0.1 μM or 10 μM GDP for $G\alpha_{q/11}$ and $G\alpha_i$, respectively, and containing the indicated concentration of ligands. Nonspecific binding was determined in the presence of 100 μM GTPγS. Reactions were incubated for 30 min at 30°C, and were terminated by the addition of 0.5 ml of ice-cold buffer, containing 20 mM HEPES, 3 mM $MgCl_2$, 100 mM NaCl, and 0.2 mM ascorbic acid. The samples were centrifuged at 16,000×g for 15 min at 4°C, and the resulting pellets resuspended in solubilization buffer (100 mM Tris, 200 mM NaCl, 1 mM EDTA, 1.25% Nonidet P-40) plus 0.2% sodium dodecylsulfate. Samples were precleared with Pansorbin (Calbiochem), followed by immunoprecipitation with antibody to $G\alpha_{q/11}$ or $G\alpha_{i1,2,3}$ (Santa Cruz Biotechnology). Finally, the immunocomplexes were washed twice with solubilization buffer, and bound [^{35}S]GTPγS was measured by liquid-scintillation spectrometry.

Construction of Receptor Chimeras.

All PCR reactions were performed using PfuTurbo Hotstart DNA polymerase (Stratagene, La Jolla, CA) in a PTC-100 thermal cycler (MJ Research, Waltham, MA). Cycling conditions were 30 cycles of 94 C/30 sec, 55 C/30 sec and 72 C/1 min per kilobase of amplicon, with an initial denaturation/activation of 94 C/2 min and a final extension of 72 C/7 min.

HA-tagged wild type human mGluR2 and mGluR3 constructs. The rat mGluR5 signal peptide (SP)[7] along with an HA epitope tag was PCR amplified using primers NheI-HA_SP/S (5'-TTTTgctagcGAATTCCTTTCCTAAAATGG-3') and HA_SP-KpnI/A (5'-TTTTggtaccACGCGTGGCGTAGTCGGGTA-3') with pRK5 as

template. Wild type human mGluR2 and mGluR3 were amplified using primers MluI-hGRM2/S (5'-agctacgcgtAAGAAGGTGCTGACCCTGGA-3') hGRM2-XbaI/A (5'-AAtctagaTCAAAGCGATGACGTTGTCGAG-3') and KpnI-hGRM3/S (5'-acgtggtaccTTAGGGGACCATAACTTTCT-3') hGRM3-XhoI/A (5'-acgtctcgagTCACAGAGATGAGGTGGTGG-3'), respectively. The rat mGluR5 signal peptide/HA epitope fragment was digested with NheI and MluI, the human mGluR2 fragment was digested with MluI and XbaI, and were simultaneously subcloned into the NheI and XbaI sites of pcDNA3.1 (Invitrogen, Carlsbad, CA) to yield the HA-tagged mGluR2 construct. Similarly, the rat mGluR5 signal peptide/HA fragment was digested with NheI and KpnI, the human mGluR2 PCR product was digested with KpnI and XhoI, and were simultaneously subcloned into the NheI and XhoI sites of pcDNA3.1 to give the HA-tagged mGluR2 construct.

Chimeric human mGluR2 with transmembrane domain 4 and 5 from human mGluR3. Fragment of the transmembrane domain TM1 to the C terminus of the second intracellular loop of the human mGluR2 was amplified using primers hGRM2-1476/S (5'-GGACACCAGCCTCATCCCAT-3') and hGRM2i2GRM3TM4/A (5'-CAGATGAAAACCTGAGAACTAGGACTGATGAAGCGTGGCC-3'). Fragment of the TM4 through TM5 of the human mGluR3 was amplified using primers hGRM2i2GRM3TM4/S (5'-GGCCACGCTTCATCAGTCCTAGTTCTCAGGTTTTCATCTG-3') and hGRM3TM5GRM2i3/A (5'-

TTTTCGGGGCACTTGCGAGTTTTGAAGGCGTACACAGTGC-3'). The two fragments were annealed and re-amplified using primers hGRM2-1476/S and hGRM3TM5GRM2i3/A. The third intracellular loop to the carboxyl terminal of the human mGluR2 was amplified using primers hGRM3TM5GRM2i3/S (5'-GCACTGTGTACGCCTTCAAAACTCGCAAGTGCCCCGAAAA-3') and hGRM2-XbaI/A. This fragment was then annealed with the previous PCR product and re-amplified using primers hGRM2-1476/S and hGRM2-XbaI/A. To reconstitute the complete chimeric receptor, the N terminal domain of the HA-tagged wild type human mGluR2 was released using NheI and BstBI, the final PCR product was digested using BstBI and XbaI, and the two fragments were simultaneously subcloned into the NheI and XbaI sites of pcDNA3.1.

Chimeric human mGluR3 with transmembrane domain 4 and 5 from human mGluR2. Fragment of the transmembrane domain TM1 to the C terminus of the second intracellular loop of the human mGluR3 was amplified using primers hGRM3-2541/S (5'- TGAAAGTTGGTCACTGGGCA-3') and hGRM3i2GRM2TM4/A (5'-CAGATGGCCACCTGTGAGGCGGGGCTGATGAATTTTGGCC-3'). Fragment of the TM4 through TM5 of the human mGluR2 was amplified using primers hGRM3i2GRM2TM4/S (5'-GGCCAAAATTCATCAGCCCCGCCTCACAGGTGGCCATCTG-3') and hGRM2TM5GRM3i3/A (5'-TTTTCTGGGCACTTCCGCGTCTTGAAGGCATAAAGCGTGC-3'). The two fragments were annealed and re-amplified using primers hGRM3-2541/S and

hGRM2TM5GRM3i3/A. The third intracellular loop to the carboxyl terminal of the human mGluR3 was amplified using primers hGRM2TM5GRM3i3/S (5'-GCACGCTTTATGCCTTCAAGACGCGGAAGTGCCCAGAAAA-3') and hGRM3-XhoI/A. This fragment was then annealed with the previous PCR product and re-amplified using primers hGRM3-2541/S and hGRM3-XhoI/A. To reconstitute the complete chimeric receptor, the N terminal domain of the HA-tagged wild type human mGluR3 was released using NheI and PstI, the final PCR product was digested using PstI and XhoI, and the two fragments were simultaneously subcloned into the NheI and XhoI sites of pcDNA3.1.

Chimeric human mGluR3 with transmembrane domain 1 through 5 from human mGluR2. A small fragment of the N terminal domain to the beginning of TM1 of the human mGluR3 was amplified using primers hGRM3-2541/S and hGRM3NGRM2TM1/A (5'-ACAGCCCAGGCATCGCCCCAGCGGATGTAGTCCTCAGGAAGGT-3'). Fragment of the TM1 through TM5 of the human mGluR2 was amplified using primers hGRM3NGRM2TM1/S (5'-ACCTTCCTGAGGACTACATCCGCTGGGGCGATGCCTGGGCTGT-3') and hGRM2TM5GRM3i3/A. The two fragments were annealed and re-amplified using primers hGRM3-2541/S and hGRM2TM5GRM3i3/A. The third intracellular loop to the carboxyl terminal of the human mGluR3 was amplified using primers hGRM2TM5GRM3i3/S and hGRM3-XhoI/A. This fragment was then annealed with the previous PCR product and re-amplified using primers hGRM3-2541/S and hGRM3-XhoI/A. To reconstitute the complete chimeric receptor, the N

terminal domain of the HA-tagged wild type human mGluR3 was released using NheI and PstI, the final PCR product was digested using PstI and XhoI, and the two fragments were simultaneously subcloned into the NheI and XhoI sites of pcDNA3.1.

Molecular modelling. Three-dimensional molecular models of the seven transmembrane (TM) regions of 2AR and mGluR2 were built using the crystal structures of β_2-adrenergic receptor[8] and rhodopsin[9], respectively, as structural templates, and the latest version of the homology-modeling program MODELLER[10]. The use of the very recent crystal structure of β_2-adrenergic receptor to build a model of 2AR is justified by the higher sequence identity between these two receptors compared to rhodopsin, and the suitability of the rhodopsin template to build models of family C GPCRs, which includes the mGluR2, has recently been discussed in the literature[11]. The sequence alignment between the transmembrane helices of β_2-adrenergic receptor and 2AR was obtained with BLAST[12]. For mGluR2, we used the same alignment with rhodopsin as described in Binet et al. (2007)[11]. A multiple alignment of available mGluR2 and mGluR3 sequences was performed with the CLUSTALW program version 1.81[13]. Supplementary Fig. S7 shows the details of these sequence alignments in the transmembrane regions.

To build a reasonable configuration of the 2AR-mGluR2, we used the TM4,5-TM4,5 configuration deriving from atomic force microscopy of rhodopsin in native disk membranes[14] as a template for the heteromer interface between 2AR and mGluR2. This modeling was obtained with the assistance of the Insight II User

Graphical Interface (Accelrys Inc.) on a graphics workstation.

Neuronal primary culture. Primary cultures of cortical and thalamic neurons were prepared as previously described[5].

Mouse brain samples. Experiments were performed as previously described[5] on adult (8–12 weeks old) male 129S6/Sv mice. For experiments involving genetically modified mice, *htr2A+/+* or *htr2A+/-* littermates were used as controls[5,16]. Animals were housed at 12 h light/dark cycle at 23°C with food and water *ad libitum*. The Institutional Animal Use and Care Committee approved all experimental procedures at Mount Sinai School of Medicine and Columbia University.

Fluorescence *in situ* hybridization (FISH). Synthesis of modified DNA oligonucleotide probes, probe labeling, and fluorescence *in situ* hybridization was performed as previously described[5,15]. See Supplementary Table S10 for oligonucleotide probe sequences.

Quantitative real-time PCR. Quantitative real-time PCR (qRT-PCR) experiments were performed as previously described[5]. See Supplementary Tables S11 and S12 for primer pair sequences.

Behavioural Studies. Behavioural studies were performed as previously described[5,16]. Motor function was assessed using a computerized three-dimentional activity monitorin system (AccuScan Instruments). The activity monitor has 32 infrared sensor pairs with 16 along each side spaced 2.5 cm apart. The system determines motor activity based on the frequency of interruptions to infrared beams traversing the *x*, *y* and *z* planes. Total distance

(cm) travelled and vertical activity were automatically determined from the interruptions of beams in the horizontal and vertical planes, respectively.

Brain Samples. Human brains were obtained at autopsies performed in the Forensic Anatomical Institute, Bilbao, Spain. The study was developed in compliance with policies of research and ethical review boards for postmortem brain studies (Basque Institute of Legal Medicine, Spain). Deaths were subjected to retrospective searching for previous medical diagnosis and treatment using examiner's information and records of hospitals and mental health centers. After searching of *antemortem* information was fulfilled, 25 subjects who had met criteria of schizophrenia according to the Diagnostic and Statistical Manual of Mental Disorders (DSM-IV)[17] were selected. A toxicological screening for antipsychotics, other drugs and ethanol was performed on blood, urine, liver and gastric contents samples. All subjects who were drug-free before death (as revealed by the absence of prescriptions in medical histories) also gave negative results in the toxicological screening. The toxicological assays were performed at the National Institute of Toxicology, Madrid, Spain, using a variety of standard procedures including radioimmunoassay, enzymatic immunoassay, high-performance liquid chromatography and gas chromatography-mass spectrometry. Controls for the present study were chosen among the collected brains on the basis, whenever possible, of the following cumulative criteria: (1) negative medical information on the presence of neuropsychiatric disorders or drug abuse; (2) appropriate gender, age and *postmortem* delay to match each subject in the schizophrenia group; (3) sudden and unexpected death (motor

vehicle accidents); and (4) toxicological screening for psychotropic drugs with negative results except for ethanol. Tissue pH is assumed to be an indicator of agonal status[18].Thus, prolonged terminal hypoxia results in low tissular pH. It has been demonstrated that gene expression patterns are strongly dependent on tissue pH. Brief deaths, associated with accidents, cardiac events or asphyxia, generally had normal pH with minor influence on gene expression changes[19]. All schizophrenic and control subjects showed a sudden and rapid death without long agonal phase. The tissue storage period before assays did not differ between schizophrenic cases (82 ± 9 months) and controls (85 ± 10 months). Specimens of prefrontal cortex (Brodmann's area 9) were dissected at autopsy (0.5-1 g tissue) on an ice-cooled surface and immediately stored at -70°C until membrane preparation. The definitive pairs of antipsychotic-untreated schizophrenics and respective matched controls are shown in Supplementary Table S8, and the definitive pairs of antipsychotic-treated schizophrenics and respective matched controls are shown in Supplementary Table S9.

SUPPLEMENTARY FIGURE LEGENDS

Figure S1. Evaluation of the specificity of FISH assay. **a,** FISH assay for *2AR* and *β-actin* in *htr2A+/+* and *htr2A-/-* mouse SCx. Red, green, and blue colours indicate *2AR*, *β-actin*, and nucleus (DAPI), respectively. **b,** Competition of *2AR*, *mGluR2* and *mGluR3* hybridization by specific, unlabeled oligonucleotide probes. A FISH assay in mouse SCx (*2AR* and *mGluR2*) and in mouse thalamus (*mGluR3*) with the fluorescently labelled oligonucleotides used in Fig. 1 was performed with the inclusion of excess of unlabeled oligonucleotides in the hybridization buffers. The presence of specific unlabeled oligonucleotides completely eliminated the signal obtained with the fluorescently labeled oligonucleotide probes. Red, green, and blue colours indicate *2AR*, *mGluR2* or *mGluR3*, and nucleus (DAPI), respectively. **c,** Similar anatomical pattern of expression of mGluR2 in mouse SCx was obtained with two different sets of fluorescently labeled oligonucleotide probes, and with the combination of probe set 1 and probe set 2. Green, and blue colours indicate *mGluR2* and nucleus (DAPI), respectively. **d,** Evaluation of FISH assay specificity using scrambled-sequence oligonucleotide probes. FISH was performed by using a mixture of five fluorescently-labeled scrambled oligonucleotide probes. Scale bar, 500 μm. See Supplementary Table S10 for oligonucleotide sequences.

Figure S2. Lower expression of mGluR2 in the absence of cortical 2AR. **a,** Schematic representation of *htr2A+/+*, *htr2A-/-*, *htr2A-/-:Emx-Cre*, and *htr2A-/-:Htt-Cre* mice. Note that in *htr2A-/-:Emx-Cre* mice (cortical rescue), 2AR is only expressed in cortical pyramidal neurons, and in *htr2A-/-:Htt-Cre* mice (thalamic

rescue), 2AR is only expressed in thalamic neurons. **b, c,** [^{3}H]LY341495 binding saturation curves in mouse SCx membranes (n = 6 per group). B_{max} values were significantly lower in *htr2A-/-* mice ($p < 0.001$; Student's *t*-test), and in *htr2A-/-:Htt-Cre* mice ($p < 0.001$; ANOVA with Bonferroni's post hoc test). **d,** Expression of *mGluR2* and *mGluR3* mRNA in mouse SCx in *htr2A+/+* (black), *htr2A-/-* (white), *htr2A+/-* (blue), *htr2A-/-:Emx-Cre* (red), and *htr2A-/-:Htt-Cre* (green) mice assayed by qRT-PCR (n = 6-12 per group). Expression level was significantly lower for *mGluR2* in *htr2A-/-* mice ($p < 0.001$; Student's *t*-test), and in *htr2A-/-:Htt-Cre* mice ($p < 0.05$; ANOVA with Bonferroni's post hoc test).

Figure S3. Intact HEK293 cells transiently transfected with (**a**) increasing amounts of mGluR2-*R*luc or mGluR3-*R*luc or (**b**) with increasing amounts of 2AR-GFP^2, 2CR-GFP^2 or pGFP^2. The amount of each cDNA is noted. Donor (**a**) and acceptor (**b**) conjugate relative expression levels were monitored by measuring luminescence and fluorescence. Note that the signals detected are comparable for different donors and acceptors. Data from triplicates assays in a single experiment are displayed. Two further experiments produced similar results.

Figure S4. [^{3}H]Ketanserin binding displacement curves by DOI, DOM and DOB in mouse SCx membranes (top panels). Note that the affinity of DOI displacing [^{3}H]ketanserin binding was significantly higher in the presence of 10μM LY379, (see Supplementary Table S2). [^{3}H]LY341495 binding displacement curves by LY379, DCG-IV and L-CCG-I in mouse SCx membranes (bottom panels). Note that the affinity of LY379, DCG-IV and L-CCG-I displacing [^{3}H]LY341495 binding

was significantly lower in the presence of 10μM DOI (see Supplementary Table S3).

Figure S5. [^{3}H]Ketanserin binding and [^{3}H]LY341495 binding in HEK293 cells stably expressing 2AR and transfected with mock, mGluR2 or mGluR3. **a,** [^{3}H]Ketanserin binding saturation curve in HEK293 cells stably expressing 2AR. **b,** [^{3}H]LY341495 binding saturation curves in HEK293 cells stably expressing 2AR and transfected with mock (open squares), 1 μg (filled triangles), 3 μg (inverted filled triangles), 6 μg (filed diamonds) , 12 μg (filled circles), or 24 μg mGluR2-eYFP (filled squares), or 24 μg mGluR3-eYFP (opened triangles). See Supplementary Table S4 for receptor densities. Note that [^{3}H]Ketanserin and [^{3}H]LY341495 B_{max} values in mouse SCx were 572±50 fmol/mg prot. and 2986±64 fmol/mg prot., respectively, and that [^{3}H]Ketanserin and [^{3}H]LY341495 B_{max} values in cortical primary cultures were 404±12 fmol/mg prot. and 1246±34 fmol/mg prot., respectively. **c,** [^{3}H]Ketanserin binding displacement curves in HEK293 cells stably expressing 2AR and transfected with mock, 24 μg of mGluR2-eYFP (left panels), or 24 μg mGluR3-eYFP (right panels). See Supplementary Table S4 for pharmacological parameters.

Figure S6. Characterization of mGluR2/mGluR3 chimeras. **a,** N-terminally HA-tagged mGluR2, mGluR3 and mGluR2/mGluR3 chimeras were expressed in HEK293 cells, fixed and stained with anti-HA antibody. **b**, [^{3}H]LY341495 binding saturation curves in HEK293 cells transfected with mock, mGluR2, mGluR3 and mGluR2/mGluR3 chimeras. Note that the level of expression is comparable for the different constructs (see also Supplementary Fig. S5). **c,** [^{3}H]Ketanserin

binding displacement curves by DOI in HEK293 cells stably expressing 2AR and transfected with mock mGluR2, mGluR3 and mGluR2/mGluR3 chimeras. Note that the 2AR affinity for DOI was decreased by mGluR2, ΔmGluR2, mGluR3ΔTM1-5 and mGluR3ΔTM4,5 co-expression, and was unaffected by mGluR3 and mGluR2ΔTM4,5 co-expression (see also Fig. 2 and Supplementary Table S5).

Figure S7. Multiple sequence alignment of the transmembrane regions of mGluR2 and mGluR3 with those of 2AR, β_2-adrenergic receptor and rhodopsin. All residues are identified by the generic numbering system for rhodopsin-like GPCR sequences as well as by the residue numbers of the amino acidic sequences of the cloned human and rat mGluR2 (MGR2_HUMAN and MGR2_RAT, respectively), human, *Pongo pygmaeus*, mouse and rat mGluR3 (MGR3_HUMAN, MGR3_PONPY, MGR3_MOUSE, and MGR3_RAT, respectively), human 2AR (5HT2A_HUMAN), human β_2-adrenergic receptor (B2AR_HUMAN), and bovine rhodopsin (OPSD_BOVIN).

Fig S8. Double-label FISH was performed in SCx layers V and VI in mice injected (i.p.) with vehicle or 0.24 mg/kg LSD 15 min after being pre-injected with vehicle or 15 mg/kg LY379. Red, green, and blue colours indicate *2AR*, *c-fos* (**a**) or *egr-2* (**b**), and nucleus (DAPI), respectively. Note that the induction of the hallucinogen signalling marker *egr-2* is selectively attenuated by LY379 in mouse SCx. Scale bar, 60 μm.

Figure S9. Activation of mGluR2 inhibits the specific cellular responses induced by 2AR agonists in mouse SCx. Dose-response curves of LY379 on cellular

response induced by 2AR agonists in mouse SCx assayed by qRT-PCR. Mice were injected with vehicle, 2 mg/kg DOI, 4 mg/kg DOM, 1 mg/kg DOB, 0.24 mg/kg LSD, 0.4 mg/kg lisuride, or 0.5 mg/kg ergotamine 15 min after being pre-injected with vehicle or 15 mg/kg LY379 (n = 4-12 per group). Note that the induction of the hallucinogenic genomic marker *egr-2* is selectively attenuated by LY379. Data are means±s.e.m. Bonferroni's post hoc test of two-factor ANOVA. *p < 0.05, **p < 0.01, ***p < 0.001.

Figure S10. Activation of mGluR2 inhibits the specific cellular responses induced by 2AR agonists in cortical primary cultures. Cortical primary cultures were treated for 45 min with vehicle, 10 μM DOI, 10 μM LSD or 10 μM lisuride after being pre-treated for 15 min with vehicle or LY379 (n = 4-12 per group). Note that the induction of the hallucinogenic genomic marker *egr-2* is selectively attenuated by LY379. Data are means±s.e.m. Bonferroni's post hoc test of two-factor ANOVA. *p < 0.05, **p < 0.01, ***p < 0.001.

Figure S11. Head twitch response was determined in mice injected with vehicle, 2 mg/kg DOI or 0.24 mg/kg LSD 15 min after being pre-injected with 15 mg/kg LY379 (n = 5-12 per group). Data are means±s.e.m. ANOVA with Bonferroni's post hoc test. *p < 0.05, **p < 0.01, ***p < 0.001.

Figure S12. Chronic clozapine modulates the expression of the components of the 2AR/mGluR2 complex in mouse SCx. Animals were chronically (21 days) injected with vehicle (black) or 25 mg/kg clozapine (red) and sacrificed 1 day after the last clozapine injection. **a,** [^{3}H]Ketanserin binding in mouse SCx after vehicle or chronic clozapine (n = 6 per group). **b, c,** [^{3}H]LY341495 binding in

htr2A+/+ (b) or *htr2A-/-* (c) mouse SCx after vehicle or chronic clozapine (n = 6 per group). **d,** Expression of *2AR*, *mGluR2*, and *mGluR3* mRNA in mouse SCx assayed by qRT-PCR in *htr2A+/+* and *htr2A-/-* mice after vehicle or chronic clozapine (n = 6-12 per group). Data are means±s.e.m. *p < 0.05, **p < 0.01, ***p < 0.001; Student's *t*-test.

Figure S13. Chronic haloperidol does not affect the expression of the components of the 2AR/mGluR2 in mouse SCx. Animals were chronically (21 days) injected with vehicle (black) or 1 mg/kg haloperidol (red) and sacrificed 1 day after the last haloperidol injection. **a,** [^{3}H]Ketanserin binding in mouse SCx after vehicle or chronic haloperidol (n = 6 per group). **b,** [^{3}H]LY341495 binding in mouse SCx after vehicle or chronic haloperidol (n = 6 per group).

Figure S14. Age-related changes in [^{3}H]ketanserin (a, b) and [^{3}H]LY341495 (c, d) binding to cortical membranes of control subjects . **a, c,** Representative saturation curves. Data correspond to a 21-year-old subject (black) and an 86-year-old subject (white). **b, d,** [^{3}H]ketanserin (b) and [^{3}H]LY379268 (d) binding B_{max} values expressed in linear relation to the age of control subjects. Estimated linear regressions are represented. Statistical values represent Pearson's correlation coefficients between binding B_{max} values and age (n = 35).

SUPPLEMENTARY REFERENCES

1. Ebersole, B. J., Visiers, I., Weinstein, H. & Sealfon, S. C. Molecular basis of partial agonism: orientation of indoleamine ligands in the binding pocket of the human serotonin 5-HT2A receptor determines relative efficacy. *Mol Pharmacol* **63,** 36-43 (2003).
2. Gonzalez-Maeso, J. *et al.* Transcriptome fingerprints distinguish hallucinogenic and nonhallucinogenic 5-hydroxytryptamine 2A receptor agonist effects in mouse somatosensory cortex. *J Neurosci* **23,** 8836-43 (2003).
3. Lopez-Gimenez, J. F., Canals, M., Pediani, J. D. & Milligan, G. The alpha1b-adrenoceptor exists as a higher-order oligomer: effective oligomerization is required for receptor maturation, surface delivery, and function. *Mol Pharmacol* **71,** 1015-29 (2007).
4. James, J. R., Oliveira, M. I., Carmo, A. M., Iaboni, A. & Davis, S. J. A rigorous experimental framework for detecting protein oligomerization using bioluminescence resonance energy transfer. *Nat Methods* **3,** 1001-6 (2006).
5. Gonzalez-Maeso, J. *et al.* Hallucinogens Recruit Specific Cortical 5-HT(2A) Receptor-Mediated Signaling Pathways to Affect Behavior. *Neuron* **53,** 439-52 (2007).
6. Wright, R. A., Arnold, M. B., Wheeler, W. J., Ornstein, P. L. & Schoepp, D. D. [3H]LY341495 binding to group II metabotropic glutamate receptors in rat brain. *J Pharmacol Exp Ther* **298,** 453-60 (2001).

7. Blahos, J., 2nd *et al.* Extreme C terminus of G protein alpha-subunits contains a site that discriminates between Gi-coupled metabotropic glutamate receptors. *J Biol Chem* **273,** 25765-9 (1998).

8. Cherezov, V. *et al.* High-resolution crystal structure of an engineered human beta2-adrenergic G protein-coupled receptor. *Science* **318,** 1258-65 (2007).

9. Li, J., Edwards, P. C., Burghammer, M., Villa, C. & Schertler, G. F. Structure of bovine rhodopsin in a trigonal crystal form. *J Mol Biol* **343,** 1409-38 (2004).

10. Sali, A. & Blundell, T. L. Comparative protein modelling by satisfaction of spatial restraints. *J Mol Biol* **234,** 779-815 (1993).

11. Binet, V. *et al.* Common structural requirements for heptahelical domain function in class A and class C G protein-coupled receptors. *J Biol Chem* **282,** 12154-63 (2007).

12. Altschul, S. F., Gish, W., Miller, W., Myers, E. W. & Lipman, D. J. Basic local alignment search tool. *J Mol Biol* **215,** 403-10 (1990).

13. Thompson, J. D., Higgins, D. G. & Gibson, T. J. CLUSTAL W: improving the sensitivity of progressive multiple sequence alignment through sequence weighting, position-specific gap penalties and weight matrix choice. *Nucleic Acids Res* **22,** 4673-80 (1994).

14. Liang, Y. *et al.* Organization of the G protein-coupled receptors rhodopsin and opsin in native membranes. *J Biol Chem* **278,** 21655-62 (2003).

15. Chan, P., Yuen, T., Ruf, F., Gonzalez-Maeso, J. & Sealfon, S. C. Method for multiplex cellular detection of mRNAs using quantum dot fluorescent in situ hybridization. *Nucleic Acids Res* **33,** e161 (2005).

16. Weisstaub, N. V. *et al.* Cortical 5-HT2A receptor signaling modulates anxiety-like behaviors in mice. *Science* **313,** 536-40 (2006).

17. American Psychiatric Association. Diagnostic and Statistical Manual of Mental Disorders: DSM-IV 4th edition (Washington , DC, 1994).

18. Preece, P. & Cairns, N. J. Quantifying mRNA in postmortem human brain: influence of gender, age at death, postmortem interval, brain pH, agonal state and inter-lobe mRNA variance. *Brain Res Mol Brain Res* **118,** 60-71 (2003).

19. Li, J. Z. *et al.* Systematic changes in gene expression in postmortem human brains associated with tissue pH and terminal medical conditions. *Hum Mol Genet* **13,** 609-16 (2004).

Supplementary Table S1. Relative mRNA expression levels (*htr2A-/-* over *htr2A+/+*) of metabotropic glutamate receptors in mouse SCx estimated by qRT-PCR. See Supplementary Table 12 for GenBank accession numbers and primer sequences.

Gene Name	Fold change
grm1	0.98 ± 0.07
grm2	0.75 ± 0.03*
grm3	1.03 ± 0.09
grm4	1.17 ± 0.11
grm5	0.94 ± 0.06
grm6	N.D.
grm7	0.97 ± 0.08
grm8	0.91 ± 0.07

*p<0.001, Student's *t*-test, n = 12-44. N.D., not detected

Supplementary Table S2.

[^{3}H]Ketanserin binding displacement curves by DOI in mouse SCx membranes.

Ligand	$K_{i\text{-}high}$ (log M)	$K_{i\text{-}low}$ (log M)	% High
vehicle	-8.9 ± 0.2	-6.8 ± 0.07	20 ± 3
LY379 0.1μM	-8.9 ± 0.3	-6.7 ± 0.08	19 ± 4
LY379 1μM	-9.4 ± 0.3	-6.7 ± 0.09	26 ± 4
LY379 10μM	-9.7 ± 0.2*	-6.7 ± 0.06	23 ± 3
LY379 10μM + LY34	-8.8 ± 0.2	-6.6 ± 0.07	20 ± 3
GTPγS	NA	-6.8 ± 0.05	NA

DOI displacement of [^{3}H]ketanserin (2 nM; K_D = 2.72 nM) binding was performed in the absence (vehicle) or in the presence of LY379, LY34 (1 μM) or GTPγS (10 μM). Competition curves were analysed by nonlinear regression to derive dissociation constants for the high- ($K_{i\text{-}high}$), and the low- ($K_{i\text{-}low}$) affinity states of the receptor. % High refers to the percentage of high-affinity binding sites as calculated from nonlinear fitting. Values are best fit ± S.E. of 3-6 experiments performed in duplicate. One-site model or two-site model as a better description of the data was determined by *F* test. Two-site model, $p < 0.001$. NA, two-site model not applicable ($p > 0.05$). DOI displacement curve of [^{3}H]ketanserin with 10 μM LY379 compared to DOI displacement curve of [^{3}H]ketanserin with vehicle: $F[5,268] = 4.97$, *$p < 0.001$.

[^{3}H]Ketanserin binding displacement curves by DOM in mouse SCx membranes.

Ligand	$K_{i\text{-}high}$ (log M)	$K_{i\text{-}low}$ (log M)	% High
vehicle	-8.1 ± 0.3	-6.2 ± 0.09	18 ± 5
LY379 0.1μM	-8.4 ± 0.3	-6.1 ± 0.11	23 ± 8
LY379 1μM	-8.5 ± 0.1	-6.0 ± 0.07	29 ± 2*
LY379 10μM	-8.7 ± 0.2	-6.0 ± 0.06	32 ± 2**
LY379 10μM + LY34	-8.4 ± 0.4	-6.2 ± 0.11	17 ± 4
GTPγS	NA	-6.4 ± 0.07	NA

DOM displacement of [^{3}H]ketanserin (2 nM; K_D = 2.72 nM) binding was performed in the absence (vehicle) or in the presence of LY379, LY34 (1 μM) or GTPγS (10 μM). Competition curves were analysed by nonlinear regression to derive dissociation constants for the high- ($K_{i\text{-}high}$), and the low- ($K_{i\text{-}low}$) affinity states of the receptor. % High refers to the percentage of high-affinity binding sites as calculated from nonlinear fitting. Values are best fit ± S.E. of 3 experiments performed in duplicate. One-site model or two-site model as a better description of the data was determined by *F* test. Two-site model, $p < 0.001$. NA, two-site model not applicable ($p > 0.05$). DOM displacement curve of [^{3}H]ketanserin with 1 μM LY379 compared to DOM displacement curve of [^{3}H]ketanserin with vehicle: $F[5,155] = 12.24$, *$p < 0.001$. DOM displacement curve of [^{3}H]ketanserin with 10 μM LY379 compared to DOM displacement curve of [^{3}H]ketanserin with vehicle: $F[5,155] = 17.7$, **$p < 0.001$.

[^{3}H]Ketanserin binding displacement curves by DOB in mouse SCx membranes.

Ligand	$K_{i\text{-}high}$ (log M)	$K_{i\text{-}low}$ (log M)	% High
vehicle	-8.2 ± 0.2	-6.3 ± 0.08	33 ± 3
LY379 0.1μM	-9.0 ± 0.2*	-6.3 ± 0.07	30 ± 3
LY379 1μM	-9.0 ± 0.3**	-6.3 ± 0.11	33 ± 4
LY379 10μM	-9.3 ± 0.1***	-6.4 ± 0.07	33 ± 2
LY379 10μM + LY34	-8.1 ± 0.3	-6.4 ± 0.14	31 ± 7
GTPγS	NA	-6.1 ± 0.07	NA

DOB displacement of [^{3}H]ketanserin (2 nM; K_D = 2.72 nM) binding was performed in the absence (vehicle) or in the presence of LY379, LY34 (1 μM) or GTPγS (10 μM). Competition curves were analysed by nonlinear regression to derive dissociation constants for the high- ($K_{i\text{-}high}$), and the low- ($K_{i\text{-}low}$) affinity states of the receptor. % High refers to the percentage of high-affinity binding sites as calculated from nonlinear fitting. Values are best fit ± S.E. of 3 experiments performed in duplicate. One-site model or two-site model as a better description of the data was determined by *F* test. Two-site model, $p < 0.001$. NA, two-site model not applicable ($p > 0.05$).). DOB displacement curve of [^{3}H]ketanserin with 0.1 μM LY379 compared to DOB displacement curve of [^{3}H]ketanserin with vehicle: $F[5,142] = 4.57$, *$p < 0.001$. DOB displacement curve of [^{3}H]ketanserin with 1 μM LY379 compared to DOB displacement curve of [^{3}H]ketanserin with vehicle: $F[5,155] = 2.67$, **$p < 0.05$. DOB displacement curve of [^{3}H]ketanserin with 10 μM LY379 compared to DOB displacement curve of [^{3}H]ketanserin with vehicle: $F[5,155] = 11.39$, ***$p < 0.001$.

Supplementary Table S3

[^{3}H]LY341495 binding displacement curves by LY379 in mouse SCx membranes.

Ligand	$K_{i\text{-}high}$ (log M)	$K_{i\text{-}low}$ (log M)	% High
vehicle	-9.3 ± 0.2	-7.4 ± 0.04	19 ± 2
DOI 0.1μM	-9.4 ± 0.5	-7.5 ± 0.07	12 ± 4
DOI 1μM	NA	-7.6 ± 0.04	NA
DOI 10μM	NA	-7.6 ± 0.02	NA
DOI 10μM + ketanserin	-9.0 ± 0.3	-7.3 ± 0.06	18 ± 5
GTPγS	-8.6 ± 0.3	-7.3 ± 0.05	14 ± 5*

LY379 displacement of [^{3}H]LY341495 (2.5 nM; K_D = 2.11 nM) binding was performed in the absence (vehicle) or in the presence of DOI, ketanserin (1 μM) or GTPγS (10μM). Competition curves were analysed by nonlinear regression to derive dissociation constants for the high- ($K_{i\text{-}high}$), and the low- ($K_{i\text{-}low}$) affinity states of the receptor. % High refers to the percentage of high-affinity binding sites as calculated from nonlinear fitting. Values are best fit ± S.E. of 3-6 experiments performed in duplicate. One-site model or two-site model as a better description of the data was determined by *F* test. Two-site model, $p < 0.001$. NA, two-site model not applicable ($p > 0.05$). LY379 displacement curve of [^{3}H]LY341495 with GTPγS compared to LY379 displacement curve of [^{3}H]LY341495 with vehicle: $F[5,88] = 12.20$, *$p < 0.001$.

[^{3}H]LY341495 binding displacement curves by DCG-IV in mouse SCx membranes.

Ligand	$K_{i\text{-}high}$ (log M)	$K_{i\text{-}low}$ (log M)	% High
vehicle	-9.5 ± 0.2	-6.4 ± 0.04	14 ± 2
DOI 0.1μM	-9.1 ± 0.6	-6.4 ± 0.06	8 ± 3
DOI 1μM	NA	-6.2 ± 0.05	NA
DOI 10μM	NA	-6.3 ± 0.05	NA
DOI 10μM + ketanserin	-9.7 ± 0.6	-6.4 ± 0.07	12 ± 4
GTPγS	NA	-6.3 ± 0.06	NA

DCG-IV displacement of [^{3}H]LY341495 (2.5 nM; K_D = 2.11 nM) binding was performed in the absence (vehicle) or in the presence of DOI, ketanserin (1 μM) or GTPγS (10μM). Competition curves were analysed by nonlinear regression to derive dissociation constants for the high- ($K_{i\text{-}high}$), and the low- ($K_{i\text{-}low}$) affinity states of the receptor. % High refers to the percentage of high-affinity binding sites as calculated from nonlinear fitting. Values are best fit ± S.E. of 3 experiments performed in duplicate. One-site model or two-site model as a better description of the data was determined by *F* test. Two-site model, $p < 0.001$. NA, two-site model not applicable ($p > 0.05$).

[^{3}H]LY341495 binding displacement curves by L-CCG-I in mouse SCx membranes.

Ligand	$K_{i\text{-}high}$ (log M)	$K_{i\text{-}low}$ (log M)	% High
vehicle	NA	-6.0 ± 0.07	NA
DOI 0.1μM	NA	-5.8 ± 0.06	NA
DOI 1μM	NA	-5.1 ± 0.13*	NA
DOI 10μM	NA	-4.9 ± 0.08**	NA
DOI 10μM + ketanserin	NA	-6.0 ± 0.09	NA
GTPγS	NA	-5.1 ± 0.09***	NA

L-CCG-I displacement of [^{3}H]LY341495 (2.5 nM; K_D = 2.11 nM) binding was performed in the absence (vehicle) or in the presence of DOI, ketanserin (1 μM) or GTPγS (10μM). Competition curves were analysed by nonlinear regression to derive dissociation constants for the high- ($K_{i\text{-}high}$), and the low- ($K_{i\text{-}low}$) affinity states of the receptor. % High refers to the percentage of high-affinity binding sites as calculated from nonlinear fitting. Values are best fit ± S.E. of 3 experiments performed in duplicate. One-site model or two-site model as a better description of the data was determined by *F* test. Two-site model, $p < 0.001$. NA, two-site model not applicable ($p > 0.05$). L-CCG-I displacement curve of [^{3}H]LY341495 with 1 μM DOI compared to L-CCG-I displacement curve of [^{3}H]LY341495 with vehicle: $F[3,78] = 56.49$, *$p < 0.001$. L-CCG-I displacement curve of [^{3}H]LY341495 with 10 μM DOI compared to L-CCG-I displacement curve of [^{3}H]LY341495 with vehicle: $F[3,78] = 51.82$, **$p < 0.001$. L-CCG-I displacement curve of [^{3}H]LY341495 with GTPγS compared to L-CCG-I displacement curve of [^{3}H]LY341495 with vehicle: $F[3,64] = 24.34$, **$p < 0.001$.

Supplementary S4. [^{3}H]Ketanserin binding displacement curves by DOI in HEK293 cell membranes stably expressing 2AR.

mGluR	Ligand	$K_{i\text{-}high}$ (log M)	$K_{i\text{-}low}$ (log M)	% High
mock	vehicle	-8.9 ± 0.2	-7.1 ± 0.2	35 ± 9
mock	GTPγS	NA	-6.7 ± 0.0	NA
mGluR2 (646 fmol/mg prot)	vehicle	-9.1 ± 0.3	-7.1 ± 0.1	30 ± 8
mGluR2 (1343 fmol/mg prot)	vehicle	-9.1 ± 0.4	-7.1 ± 0.2	28 ± 3
mGluR2 (1994 fmol/mg prot)	vehicle	NA	-7.7 ± 0.1	NA
mGluR2 (2800 fmol/mg prot)	vehicle	NA	-7.1 ± 0.0	NA
mGluR2 (3587 fmol/mg prot)	vehicle	NA	-7.4 ± 0.0	NA
mGluR2 (3587 fmol/mg prot)	LY379	-9.5 ± 0.1	-7.4 ± 0.1	28 ± 5
mGluR3 (4185 fmol/mg prot)	vehicle	-9.3 ± 0.2	-7.2 ± 0.1	29 ± 4
mGluR3 (4185 fmol/mg prot)	LY379	-9.3 ± 0.4	-7.3 ± 0.1	25 ± 5

DOI displacement of [^{3}H]ketanserin (2 nM; K_D = 0.37 nM) binding was performed in HEK293 cells stably expressing 2AR (504 ± 25 fmol/mg prot) and transfected with mock, mGluR2 or mGluR3 in the absence (vehicle) or in the presence of LY379 (10 μM). HEK293 cells were expressing different densities of mGluR2 or mGluR3 (see Supplementary Fig. S4). Competition curves were analysed by nonlinear regression to derive dissociation constants for the high- ($K_{i\text{-}high}$), and the low- ($K_{i\text{-}low}$) affinity states of the receptor. % High refers to the percentage of high-affinity binding sites as calculated from nonlinear fitting. Values are best fit ± S.E. of three experiments performed in triplicate. One-site model or two-site model as a better description of the data was determined by *F* test. Two-site model, $p < 0.001$. NA, two-site model not applicable ($p > 0.05$).

Supplementary Table S5. [^{3}H]Ketanserin binding displacement curves by DOI in HEK293 cell membranes stably expressing 2AR.

mGluR	$K_{i\text{-}high}$ (log M)	$K_{i\text{-}low}$ (log M)	% High
mock	-9.2 ± 0.3	-7.2 ± 0.1	30 ± 7
mGluR2	NA	-7.2 ± 0.0	NA
mGluR3	-9.3 ± 0.2	-7.4 ± 0.1	24 ± 7
ΔmGluR2	NA	-7.5 ± 0.1	NA
mGluR2ΔTM4,5	-9.2 ± 0.2	-6.9 ± 0.2	33 ± 9
mGluR3ΔTM1-5	NA	-7.4 ± 0.0	NA
mGluR3ΔTM4,5	NA	-7.3 ± 0.0	NA

DOI displacement of [^{3}H]ketanserin (2 nM; K_D = 0.37 nM) binding was performed in HEK293 cells stably expressing 2AR (504 ± 25 fmol/mg prot) and transfected with mock, mGluR2, mGluR3 or mGluR2/mGluR3 chimeras (See Supplementary Fig. S5). Competition curves were analysed by nonlinear regression to derive dissociation constants for the high- ($K_{i\text{-}high}$), and the low- ($K_{i\text{-}low}$) affinity states of the receptor. % High refers to the percentage of high-affinity binding sites as calculated from nonlinear fitting. Values are best fit ± S.E. of three experiments performed in triplicate. One-site model or two-site model as a better description of the data was determined by *F* test. Two-site model, $p < 0.001$. NA, two-site model not applicable ($p > 0.05$).

Supplementary Table S6. DOI-stimulated [^{35}S]GTPγS binding followed by immunoprecipitation with anti-G$\alpha_{q/11}$ antibody in HEK293 cell membranes stably expressing 2AR.

mGluR	Ligand	E_{max}	$EC_{50\text{-}high}$ (log M)	log $EC_{50\text{-}low}$ (log M)	% High
mock	vehicle	212 ± 19	-8.4 ± 0.7	-5.1 ± 0.4	39 ± 12
mGluR2	vehicle	221 ± 12	NA	-6.1 ± 0.2	NA
mGluR2	LY379	218 ± 10	-7.6 ± 0.3	-5.0 ± 0.1	40 ± 7
mGluR3	vehicle	215 ± 8	-8.4 ± 0.2	-5.0 ± 0.1	38 ± 4
mGluR3ΔTM4,5	vehicle	225 ± 10	NA	-5.9 ± 0.1	NA

[^{35}S]GTPγS binding followed by immunoprecipitation with anti-G$\alpha_{q/11}$ antibody in HEK293 cells stably expressing 2AR and transfected with mock, mGluR2, mGluR2 or mGluR3ΔTM4,5. [^{35}S]GTPγS binding was performed in the presence or in the absence of LY379 (10 μM). Concentration-response curves were analysed by nonlinear regression to derive constants for efficacy (E_{max}, % over basal [^{35}S]GTPγS binding) and high- ($EC_{50\text{-}high}$) and low- ($EC_{50\text{-}low}$) potencies for DOI. % High refers to the percentage of high-potency binding sites as calculated from nonlinear fitting. Basal binding for nonlinear regression was the [^{35}S]GTPγS binding to G$\alpha_{q/11}$ protein in the absence of DOI for each experimental condition. Values are best fit ± S.E. of three experiments performed in duplicate. Monophasic model or biphasic concentration-response model as a better description of the data was determined by *F* test. Biphasic model, $p < 0.05$, $p < 0.001$, and $p < 0.001$ for mock/vehicle, mGluR2/LY379 and mGluR3/vehicle curves, respectively. NA, biphasic model not applicable ($p > 0.05$). DOI activating G$\alpha_{q/11}$ in cortical primary cultures (see Fig. 3a): pEC_{50} vehicle, -6.7±0.1; $pEC_{50\text{-}high}$ LY379, -7.6±0.4; and $pEC_{50\text{-}low}$ LY379, -5.0±0.3 ($F[3,57] = 4.61$, $p < 0.01$).

Supplementary Table S7. DOI-stimulated [^{35}S]GTPγS binding followed by immunoprecipitation with anti-G$\alpha_{i1,2,3}$ antibody in HEK293 cell membranes stably expressing 2AR.

mGluR2	Ligand	E_{max}	log $EC_{50\text{-}high}$	log $EC_{50\text{-}low}$	% High
mock	vehicle	16.8 ± 2	NA	-4.8 ± 0.3	NA
mGluR2	vehicle	22.8 ± 1**	NA	-6.9 ± 0.2*	NA
mGluR2	LY379	11.9 ± 1	NA	-4.9 ± 0.3	NA
mGluR3	vehicle	14.07 ± 1	NA	-4.6 ± 0.3	NA
mGluR3ΔTM4,5	vehicle	24.73 ± 1***	NA	-6.4 ± 0.3***	NA

[^{35}S]GTPγS binding followed by immunoprecipitation with anti-G$\alpha_{i1,2,3}$ antibody in HEK293 cells stably expressing 2AR and transfected with mock, mGluR2, mGluR2 or mGluR3ΔTM4,5. [^{35}S]GTPγS binding was performed in the presence or in the absence of LY379 (10 μM). Concentration-response curves were analysed by nonlinear regression to derive constants for efficacy (E_{max}, % over basal [^{35}S]GTPγS binding) and high- ($EC_{50\text{-}high}$) and low- ($EC_{50\text{-}low}$) potencies for DOI. % High refers to the percentage of high-potency binding sites as calculated from nonlinear fitting. Basal binding for nonlinear regression was the [^{35}S]GTPγS binding to G$\alpha_{i1/2/3}$ protein in the absence of DOI for each experimental condition. Values are best fit ± S.E. of three experiments performed in duplicate. Monophasic concentration-response model provided a better description of the data as determined by *F* test. NA, biphasic model not applicable ($p > 0.05$). DOI concentration-response curve with mGluR2/vehicle compared to DOI concentration-response curve with mock/vehicle: $F[3,90] = 19.57$, *$p < 0.001$. DOI concentration-response curve with mGluR2/vehicle compared to DOI-concentration response curve with mGluR2/LY379: $F[3,91] = 30.70$, ** $p < 0.001$. DOI concentration-response curve with mGluR2/vehicle compared to DOI-concentration response curve with mGluR3ΔTM4,5/vehicle: $F[3,75] = 6.25$, *** $p < 0.001$. DOI activating G$\alpha_{i1,2,3}$ in cortical primary cultures (see Fig. 3a): pEC_{50} vehicle, -6.1±0.1; pEC_{50} LY379, -4.3±0.2 ($F[3,84] = 50.82$, $p < 0.001$).

Supplementary Table S8. Demographic characteristics and *antemortem* diagnoses of cases of nontreated schizophrenic subjects, and their respective control subjects.

	Gender (F/M)	Age at death (years)	Postmortem delay (h)	Antipsychotic treatment	Additional drugs
Schizophrenic 1	M	41	41	Untreated	BDZ
Control 1	M	41	24		
Schizophrenic 2	M	49	41	Untreated	
Control 2	M	49	17		
Schizophrenic 3	M	24	45	Untreated	
Control 3	M	25	42		
Schizophrenic 4	M	44	31	Untreated	BDZ; CBZ
Control 4	M	45	30		
Schizophrenic 5	F	39	11	Untreated	
Control 5	F	35	8		
Schizophrenic 6	M	43	19	Untreated	
Control 6	M	48	16		
Schizophrenic 7	M	21	24	Untreated	
Control 7	M	21	16		
Schizophrenic 8	M	23	43	Untreated	
Control 8	M	23	27		
Schizophrenic 9	M	33	36	Untreated	BDZ
Control 9	M	33	41		
Schizophrenic 10	M	31	14	Untreated	BDZ
Control 10	M	31	59		
Schizophrenic 11	M	41	16	Untreated	
Control 11	M	40	12		
Schizophrenic 12	F	25	19	Untreated	
Control 12	F	30	15		
Schizophrenic 13	M	30	13	Untreated	CC
Control 13	M	27	10		
Schizophrenia group	2F/11M	34 ± 3	27 ± 4		
Control group	2F/11M	34 ± 3	24 ± 4		

Antipsychotics were not detected in blood samples of schizophrenics. All schizophrenic subjects included, except schizophrenic 5 and schizophrenic 6, committed suicide. Abbreviations: benzodiazepines (BDZ), carbamazepine (CBZ), and cocaine (CC).

Supplementary Table S9. Demographic characteristics and *antemortem* diagnoses of cases of antipsychotic-treated schizophrenic subjects, and their respective control subjects.

	Gender (F/M)	Age at death (years)	Postmortem delay (h)	Antipsychotic treatment	Additional drugs
Schizophrenic 14	M	66	57	OLA	
Control 14	M	66	50		
Schizophrenic 15	F	30	17	HAL	BDZ; TRA
Control 15	F	29	31		
Schizophrenic 16	M	57	19	QUE	
Control 16	M	58	19		ETH (0.99 g/l)
Schizophrenic 17	M	56	8	QUE	BDZ
Control 17	M	55	15		
Schizophrenic 18	M	37	11	OLA	BDZ
Control 18	M	36	14		ETH (0.3 g/l)
Schizophrenic 19	F	35	3	QUE	BDZ
Control 19	F	35	22		
Schizophrenic 20	F	56	13	CLZ	FUR
Control 20	F	52	64		
Schizophrenic 21	M	44	6	CLT; LEV	BIP; BDZ
Control 21	M	42	9		
Schizophrenic 22	M	30	18	OLA	
Control 22	M	30	11		
Schizophrenic 23	M	32	8	QUE	BDZ; PAR
Control 23	M	32	27		AMP; ETH (0.68 g/l)
Schizophrenic 24	M	27	17	CLZ	
Control 24	M	30	10		
Schizophrenic 25	M	43	65	CLZ	
Control 25	M	38	59		
Schizophrenia group	3F/9M	43 ± 4	20 ± 6		
Control group	3F/9M	42 ± 4	28 ± 6		

Therapeutic levels of olanzapine (OLA), haloperidol (HAL), quetiapine (QUE), clozapine (CLZ), clotiapine (CLT), and levomepromazine (LEV) were detected in blood samples of schizophrenics. All schizophrenic subjects included, except schizophrenic 21 and schizophrenic 25, committed suicide. Abbreviations: benzodiazepines (BDZ), trazodone (TRA), furosemide (FUR), biperiden (BIP), amphetamine (AMP), and paracetamol (PAR). Ethanol in blood is coded as ETH.

Supplementary Table S10. Oligonucleotide probe sequences for FISH

htr2A
A**T**CCCTGGAGT**T**GAAGTCATTAGGG**T**AGAGCCTCGAG**T**CGTCACCTAA**T**T
T**T**CTGTTCTCCT**T**GTACTGGCAC**T**GAATGTACCG**T**GAGAAGGCGGACC**T**A
TTTCCACATCAGAAA**T**TCTCGCGGCAA**T**GACGGCATTC**T**AGCCAAGCG**T**G
CC**T**CGCTTCACAG**T**GCTAGGGAGAG**T**CCACGGCGGAGC**T**GTAAGTTC**T**CA
CCAG**T**GGGTTGACGGC**T**GAGGAGAGA**T**AACCAA**T**CCAGACAAACACAT**T**G
grm2
CA**T**GGGATGATGC**T**AGTATCCAGAG**T**CAGACCTTC**T**GCCCAGTAGCC**T**AA
ACAG**T**CAGCACAGG**T**GAACTCA**T**CCAGCCTG**T**ACTCATAGGGC**T**GACAGG
GG**T**CTTGAAGGCA**T**AGAGCG**T**GCAGAGAGCGA**T**GAGGAGCACGTTG**T**AGG
ACA**T**CGTAGTGGTC**T**GCACCCGATAA**T**CACTGGAGG**T**GACGTAGAAGA**T**G
GC**T**CACCACGT**T**CTTCTGTGGC**T**GGAAGAGGATAATG**T**GCAGCTTGGG**T**G
grm3
TTTGGCACTGG**T**GGAGGCGTAGCT**T**ATCTGAGGGATC**T**GGAAGAGCC**T**CA
C**T**GTCTCCCCA**T**AGTCACCT**T**CAGAGGCAACAG**T**GGACACATAGG**T**CCAG
ACAAA**T**CTGTCTGTGG**T**TTCTCTTGT**T**CTGGAGGC**T**GCACTGGAACT**T**CT
G**T**ACAACTTCTT**T**CCATCCAGGA**T**CTTCATTGCA**T**CACAGAGCTTGG**T**GG
TCATTTCAT**T**GGGGGCACAGGGATCACTGCAC**T**GGGAAGTGGGGAC**T**GAG
c-fos
TCCTCTTCAGGAGA**T**AGCTGCTCTAC**T**TTGCCCCTTC**T**GCCGATGCTC**T**G
C**T**TCAAGTTGA**T**CTGTCTCCGCT**T**GGAGTGTATCTG**T**CAGCTCCCTCC**T**C
TCCTCAGACTC**T**GGGGTGGAAGCC**T**CAGGCAGACC**T**CCAGTCAAA**T**CCAG
GA**T**GCCGGAAACAAGAAG**T**CATCAAAGGG**T**TCTGCCT**T**CAGCTCCACG**T**T
egr-2
TC**T**CCAGTCATG**T**CAATGTTGA**T**CATGCCATC**T**CCCGCCACTCCGT**T**CAT
TGGATCTCTC**T**GGCACGGAGA**T**GGAAAAAATCCAGGA**T**AGTCTGGGA**T**CA
C**T**GGTCAGCTCA**T**CAGAGCG**T**GAGAACCTCCTA**T**CACAACCTTCTGC**T**GG
TCAGAACAAC**T**GGCATCCAGGG**T**CAACGGAAAGGGC**T**AGCAGACCA**T**AGT
Scrambled
T**T**CACGGGCCTC**T**TGAAGTTGC**T**CCGGTTCAAG**T**AGCCGAAATGG**T**ACAT
G**T**GGAGTTGTCCAAG**T**CACAGTCACC**T**TGACGCTGG**T**GTATAAGAG**T**CAG
TAC**T**TGCCTCACCGCCC**T**CTACCGTAC**T**AGTTGTAAC**T**GTACTGACC**T**CT
TCCTCGTCTGTCG**T**AACACTTCAAACTG**T**GAATGCCTC**T**GCCCTACCC**T**T
G**T**GGGTTCGACG**T**GTAATAGGAGAAGG**T**CGGTGTCTTC**T**TGCACCAC**T**CG

Boldface letters represent amino-modified nucleotides, which were labeled with succinimidyl esters Alexa fluorophores.

Supplementary Table S11. Mouse qRT-PCR prime pairs

Gene Name	GenBank	Primer pairs	
		Forward	Reverse
grm1	**NM_016976**	AAGGGACAGCATGTGTGGCA	ACTCTTGCCAGAGCCTTGGT
grm2	**XM_909627**	CCATCTTCTACGTCACCTCC	AGGAACAAGCTGGGATCCAG
grm3	**NM_181850**	TGACTACAGAGTGCAGACGAC	TCGCAGTTCCACTGACACTG
grm4	**NM_00101338**	ATTGCTGCCACGCTGTTCGT	AGGAAGGTGGTGGCATAGCA
grm5	**NM_00108141**	AGCTGTGCACACAGAAGGCA	AGTGGGCGATGCAAATCCCT
grm6	**NM_173372**	ATCTTCTTTGGCACCGCCCA	TCTGCACGTTCTGCTCTGGA
grm7	**NM_177328**	TTGGCACAGCGCAATCAGCA	TGCTGTGACTACGGCCTTGA
grm8	**NM_008174**	ATGATTGCGGCACCTGACAC	TGGGATGCTGGGCTGATGAA
c-fos	**J00370**	TTCCTGGCAATAGCGTGTTC	TTCAGACCACCTCGACAATG
egr-2	**NM_000399**	TGTTAACAGGGTCTGCATGTG	AGCGGCAGTGACATTGAAG
β-actin	**X03672**	AGGTGACAGCATTGCTTCTG	GCTGCCTCAACACCTCAAC
GAPDH	**NM_008084**	TGCGACTTCAACAGCAACTC	CTTGCTCAGTGTCCTTGCTG
mapkapk5	**NM_010765**	CATTGCCCAGTGTATCCTCC	ACCTGCTTTACCACCTCTGC
rpS3	**NM_012052**	AGGTTGTGGTGTCTGGGAAG	GAGGCTTCTTGGGACCAATC

Supplementary Table S12. Human qRT-PCR prime pairs

Gene Name	GenBank	Primer pairs	
		Forward	Reverse
grm2	NM_000839	GCACAGGCAAGGAGACAGC	GAGGCAGCCAAGCACCAC
grm3	NM_000840	TCCACCCCTCCGTTTTCCC	TCATGCTAGTCCTCTCTCATTTCC
β-actin	NM_001101	GGAAATCGTGCGTGACATTAAGG	GATGGAGGGGCCGGACTC

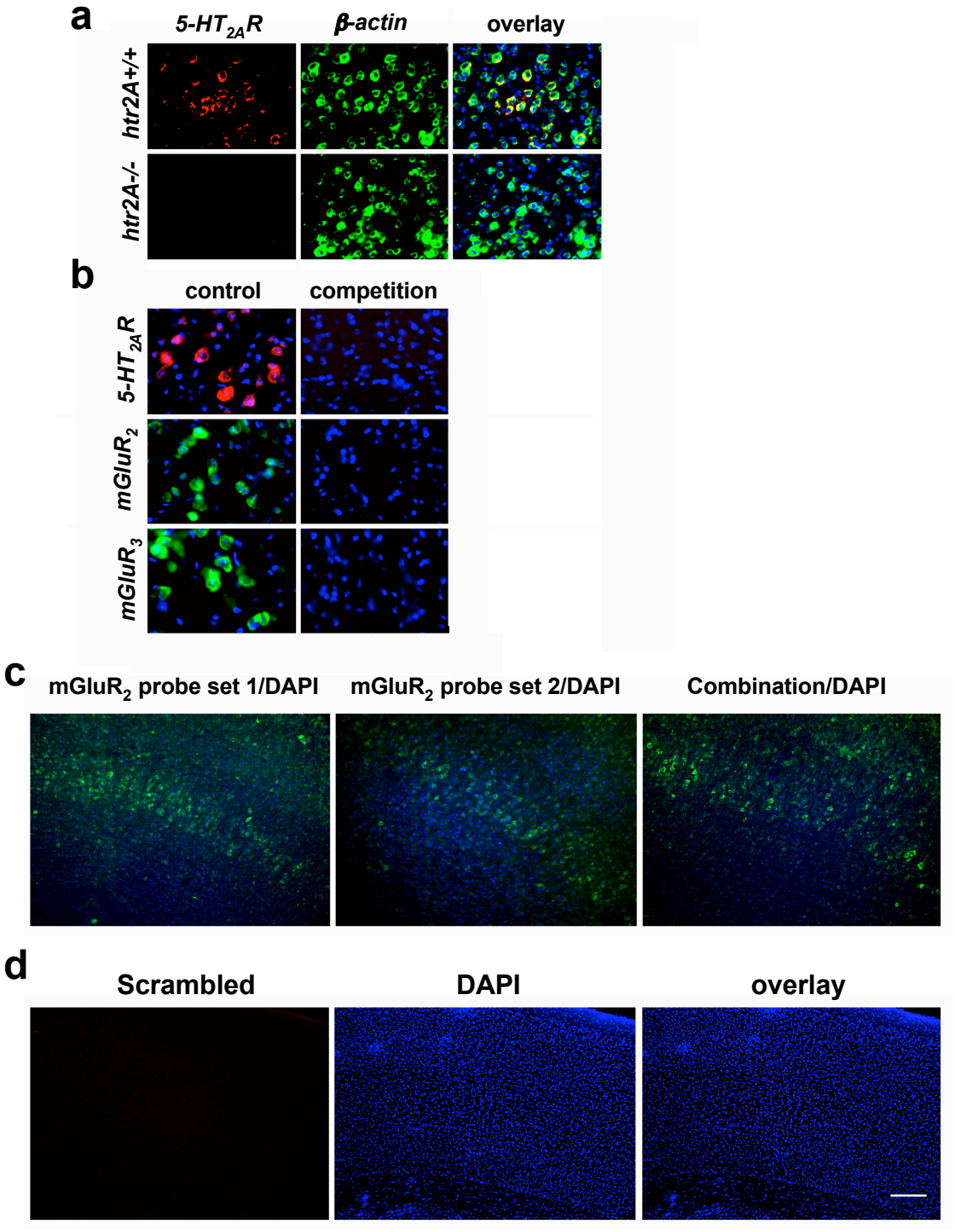

Supplementary Fig. S1

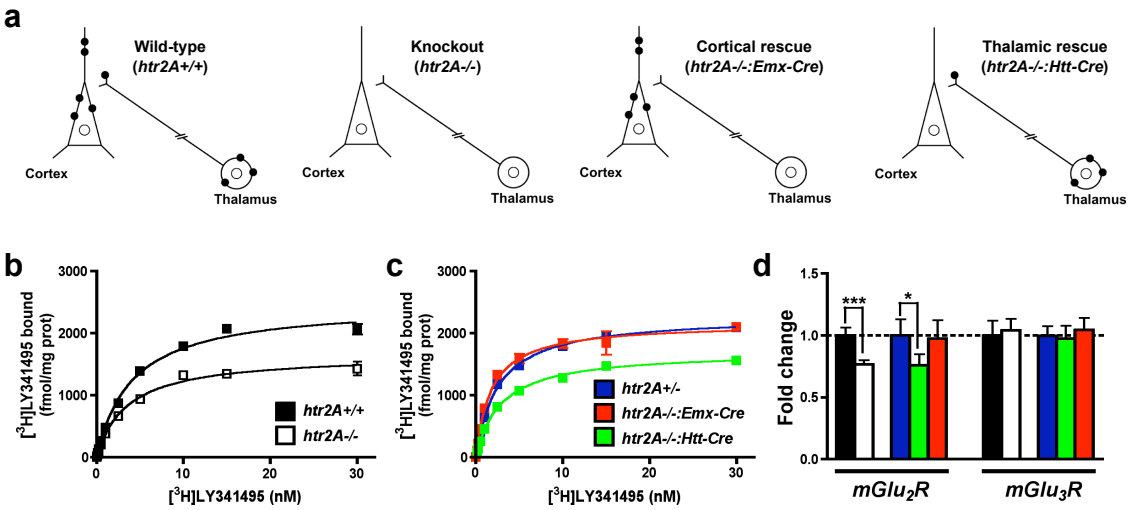

Supplementary Fig. S2

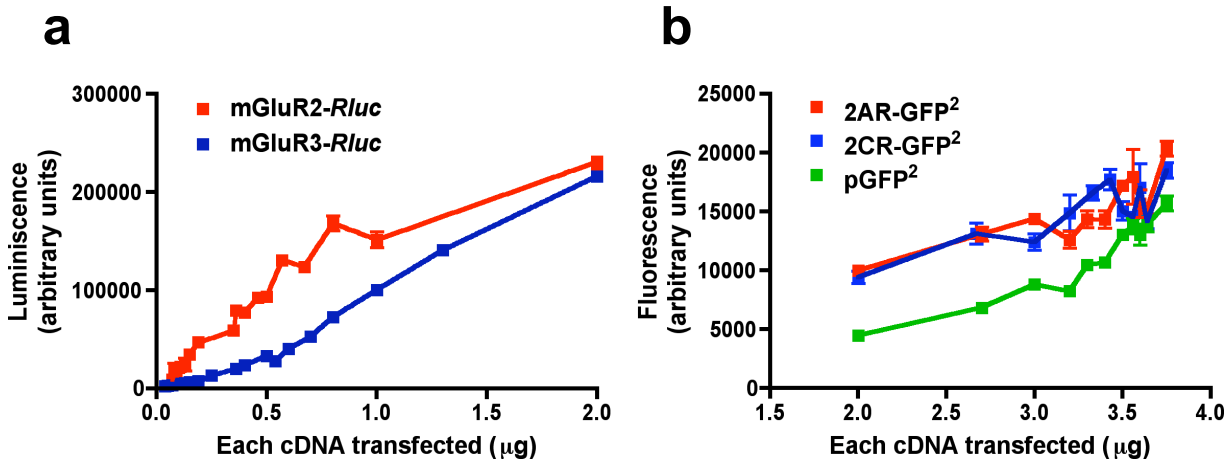

Supplementary Fig. S3

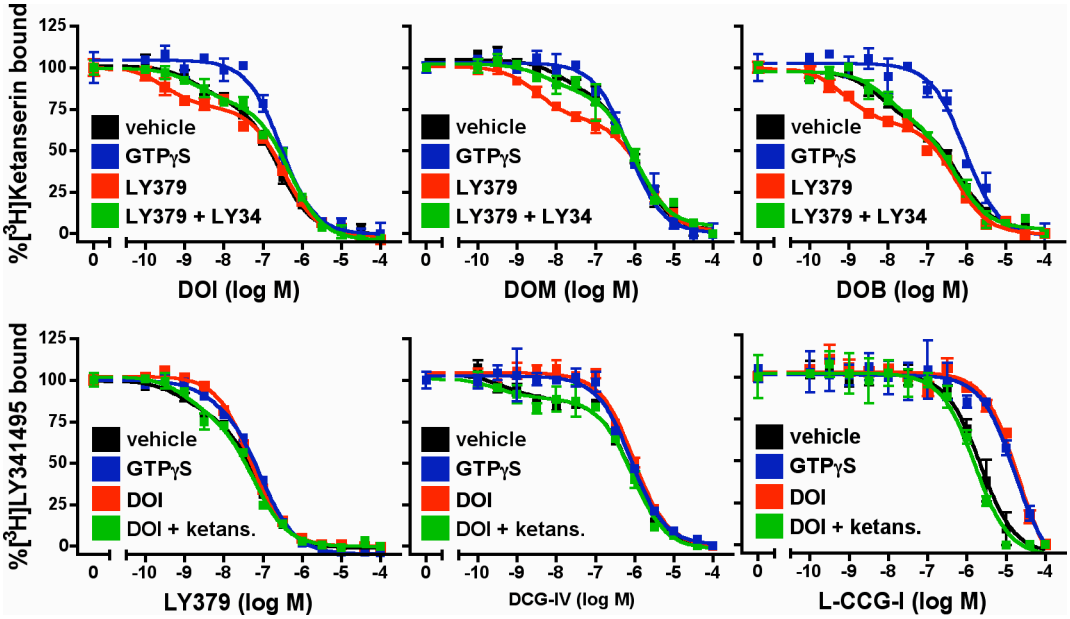

Supplementary Fig. S4

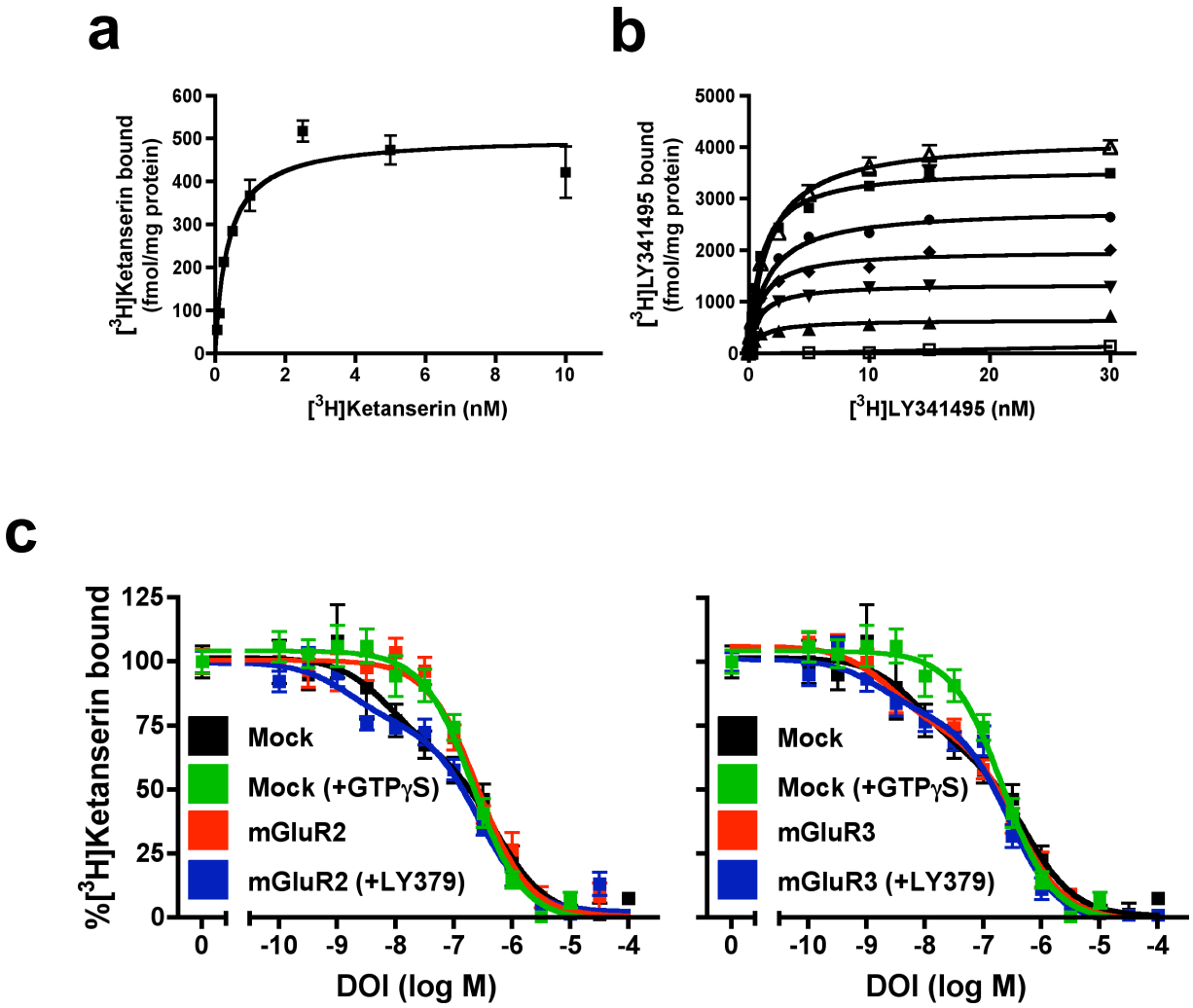

Supplementary Fig. S5

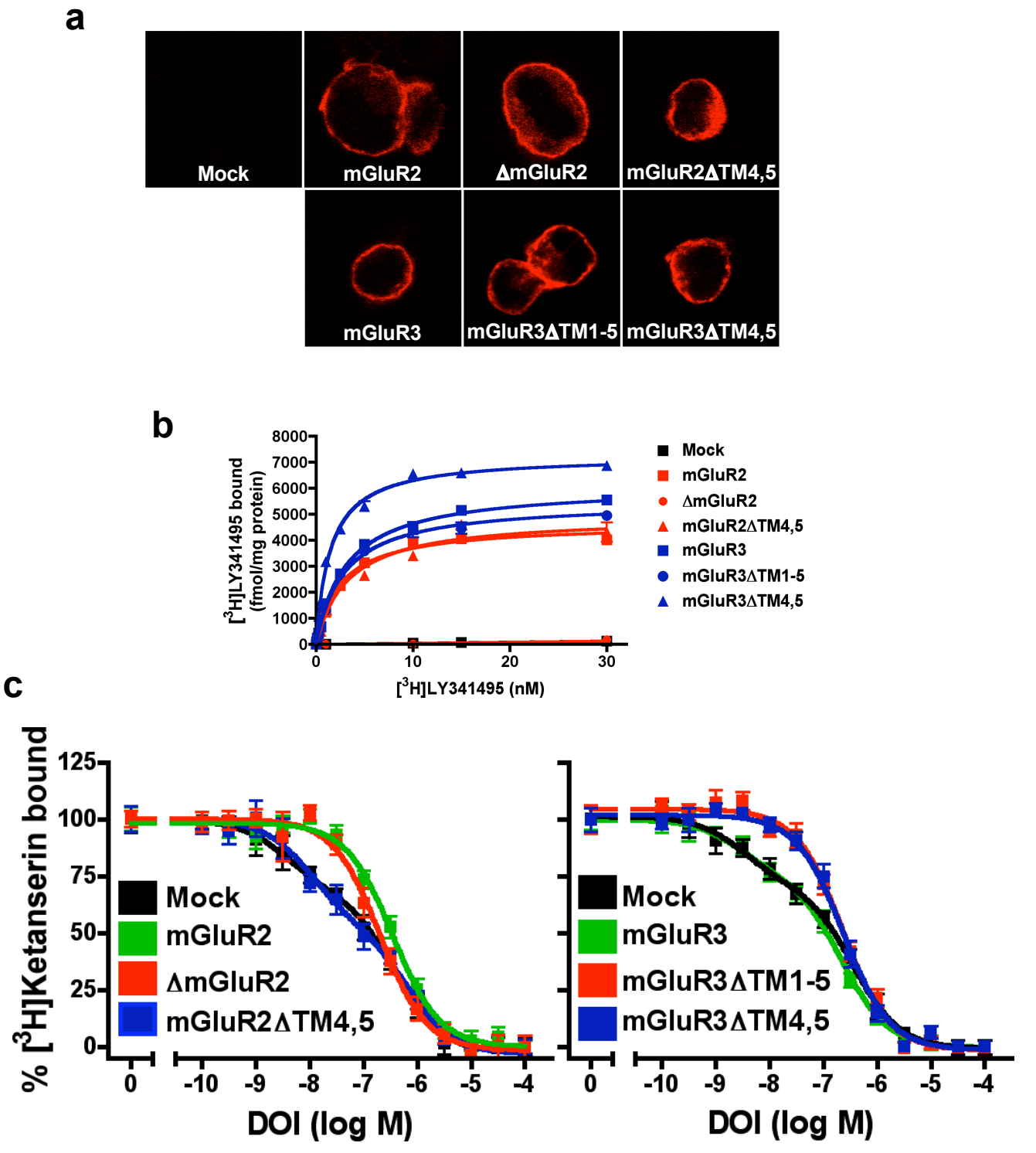

Supplementary Fig. S6

TM1	1.30	
MGR2_HUMAN	562	RWGDAWAVGPVTIACLGALATLFVLGVFVR
MGR2_RAT	562	RWGDAWAVGPVTIACLGALATLFVLGVFVR
MGR3_HUMAN	571	RWEDAWAIGPVTIACLGFMCTCMVVTVFIK
MGR3_PONPY	571	RWEDAWVIGPVTIACLGFMCTCMVVTVFIK
MGR3_MOUSE	571	RWEDAWAIGPVTIACLGFMCTCIVITVFIK
MGR3_RAT	571	KWEDAWAIGPVTIACLGFLCTCIVITVFIK
5HT2A_HUMAN	72	QEKNWSALLTAVVIILTIAGNILVIMAVSL
B2AR_HUMAN	31	VWVVGMGIVMSLIVLAIVFGNVLVITAIAK
OPSD_BOVIN	35	WQFSMLAAYMFLLIMLGFPINFLTLYVTVQ
TM2	2.38	
MGR2_HUMAN	600	ASGRELCYILLGGVFLCYCMTFIFIAK
MGR2_RAT	600	ASGRELCYILLGGVFLCYCMTFVFIAK
MGR3_HUMAN	609	ASGRELCYILLFGVGLSYCMTFFFIAK
MGR3_PONPY	609	ASGRELCYILLFGVGLSYCMTFFFIAK
MGR3_MOUSE	609	ASGRELCYILLFGVSLSYCMTFFFIAK
MGR3_RAT	609	ASGRELCYILLFGVSLSYCMTFFFIAK
5HT2A_HUMAN	108	ATNYFLMSLAIADMLLGFLVMPVSMLT
B2AR_HUMAN	67	VTNYFITSLACADLVMGLAVVPFGAAH
OPSD_BOVIN	71	PLNYILLNLAVADLFMVFGGFTTTLYT
TM3	3.22	
MGR2_HUMAN	629	TAVCTLRRLGLGTAFSVCYSALLTKTNRIARIF
MGR2_RAT	629	TAVCTLRRLGLGTAFSVCYSALLTKTNRIARIF
MGR3_HUMAN	638	PVICALRRLGLGSSFAICYSALLTKTNCIARIF
MGR3_PONPY	638	PVICALRRLGLGTSFAICYSALLTKTNCIARIF
MGR3_RAT	638	PVICALRRLGLGTSFAICYSALLTKTNCIARIF
5HT2A_HUMAN	145	SKLCAVWIYLDVLFSTASIMHLCAISLDRYVAI
B2AR_HUMAN	103	NFWCEFWTSIDVLCVTASIETLCVIAVDRYFAI
OPSD_BOVIN	107	PTGCNLEGFFATLGGEIALWSLVVLAIERYVVV
TM4	4.40	
MGR2_HUMAN	677	ASQVAICLALISGQLLIVVAWLV
MGR2_RAT	677	ASQVAICLALISGQLLIVAAWLV
MGR3_HUMAN	686	SSQVFICLGLILVQIVMVSVWLI
MGR3_PONPY	686	SSQVFICLGLILVQIVMVSVWLI
MGR3_MOUSE	686	SSQVFICLGLILVQIVMVSVWLI
MGR3_RAT	686	SSQVFICLGLILVQIVMVSVWLI
5HT2A_HUMAN	190	TKAFLKIIAVWTISVGISMPIPV
B2AR_HUMAN	148	NKARVIILMVWIVSGLTSFLPIQ
OPSD_BOVIN	151	NHAIMGVAFTWVMALACAAPPLV
TM5	5.38	
MGR2_HUMAN	726	ASMLGSLAYNVLLIALCTLYAFK
MGR2_RAT	726	ASMLGSLAYNVLLIALCTLYAFK
MGR3_HUMAN	735	SSMLISLTYDVILVILCTVYAFK
MGR3_PONPY	735	SSMLISLTYDVILVILCTVYAFK
MGR3_MOUSE	735	SSMLISLTYDVVLVILCTVYAFK
MGR3_RAT	735	SSMLISLTYDVVLVILCTVYAFK
5HT2A_HUMAN	234	FVLIGSFVSFFIPLTIMVITYFL
B2AR_HUMAN	199	YAIASSIVSFYVPLVIMVFVYSR
OPSD_BOVIN	203	FVIYMFVVHFIIPLIVIFFCYGQ
TM6	6.32	
MGR2_HUMAN	757	NEAKFIGFTMYTTCIIWLAFLPIFYVTSS
MGR2_RAT	757	NEAKFIGFTMYTTCIIWLAFLPIFYVTSS
MGR3_HUMAN	766	NEAKFIGFTMYTTCIIWLAFLPIFYVTSS
MGR3_PONPY	766	NEAKFIGFTMYTTCIIWLAFLPIFYVTSS
MGR3_MOUSE	766	NEAKFIGFTMYTTCIIWLAFLPIFYVTSS
MGR3_RAT	766	NEAKFIGFTMYTTCIIWLAFLPIFYVTSS
5HT2A_HUMAN	320	KACKVLGIVFFLFVVMWCPFFITNIMAVI
B2AR_HUMAN	270	KALKTLGIIMGTFTLCWLPFFIVNIVHVI
OPSD_BOVIN	249	EVTRMVIIMVIAFLICWLPYAGVAFYIFT
TM7	7.33	
MGR2_HUMAN	788	RVQTTTMCVSVSLSGSVVLGCLFAPKLHIILFQPQKNV
MGR2_RAT	788	RVQTTTMCVSVSLSGSVVLGCLFAPKLHIILFQPQKNV
MGR3_HUMAN	797	RVQTTTMCISVSLSGFVVLGCLFAPKVHIILFQPQKNV
MGR3_PONPY	797	RVQTTTMCISVSLSGFVVLGCLFAPKVHIILFQPQKNV
MGR3_MOUSE	797	RVQTTTMCISVSLSGFVVLGCLFAPKVHIVLFQPQKNV
MGR3_RAT	797	RVQTTTMCISVSLSGFVVLGCLFAPKVHIVLFQPQKNV
5HT2A_HUMAN	360	ALLNVFVWIGYLSSAVNPLVYTLFNKTYRSAFSRYIQC
B2AR_HUMAN	306	EVYILLNWIGYVNSGFNPLIYCR-SPDFRIAFQELLCL
OPSD_BOVIN	286	IFMTIPAFFAKTSAVYNPVIYIMMNKQFRNCMVTTLCC

Supplementary Fig. S7

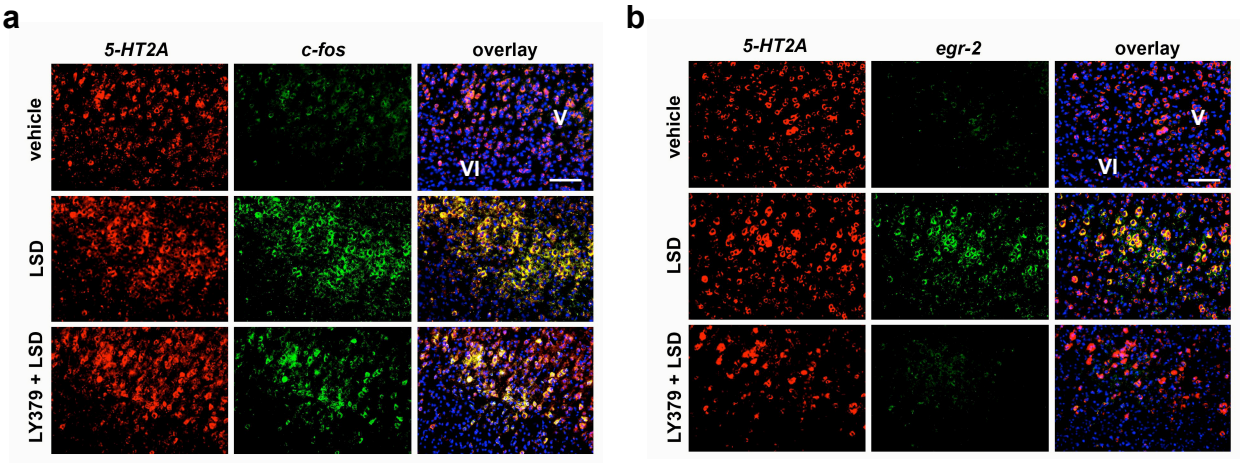

Supplementary Fig. S8

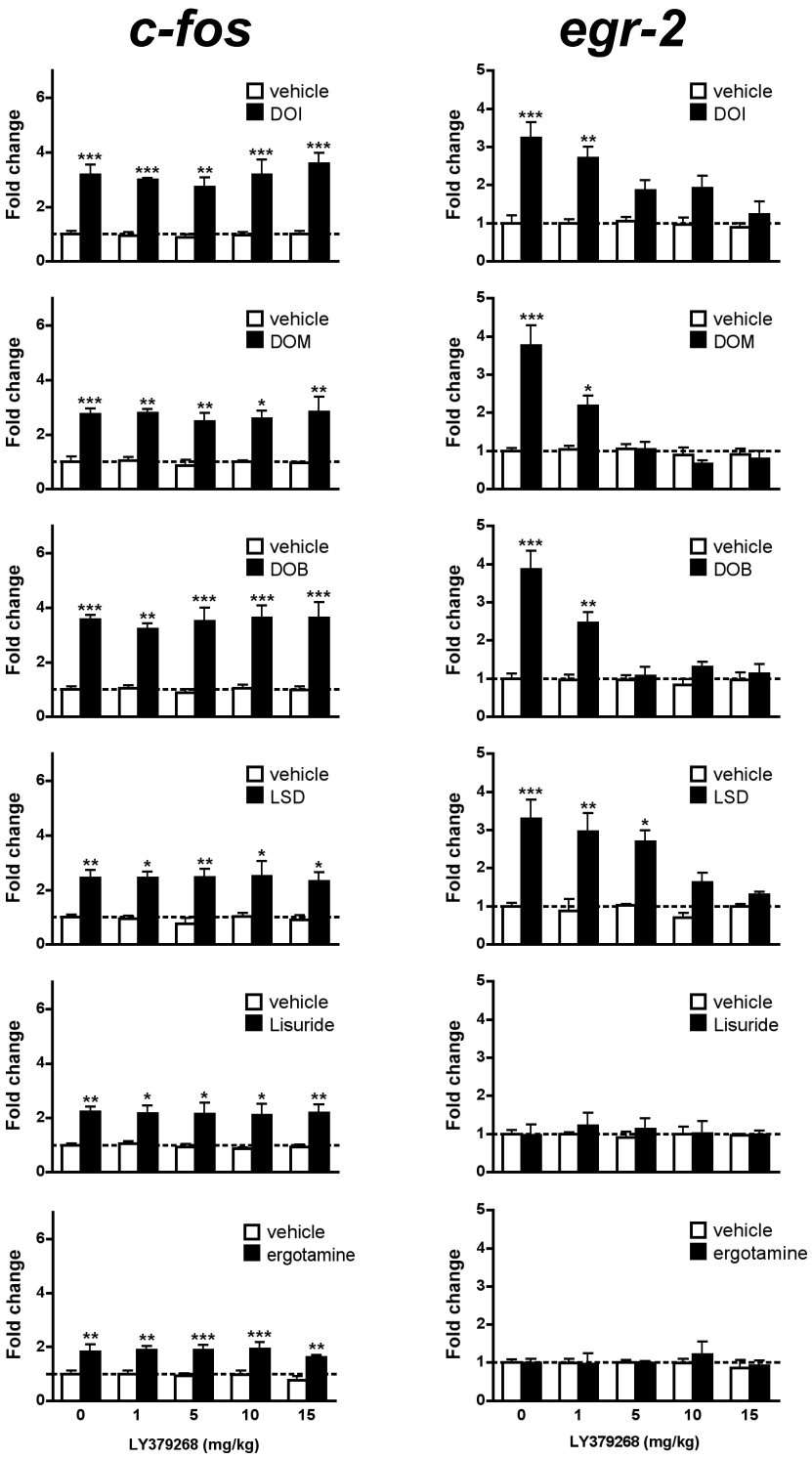

Supplementary Fig. S9

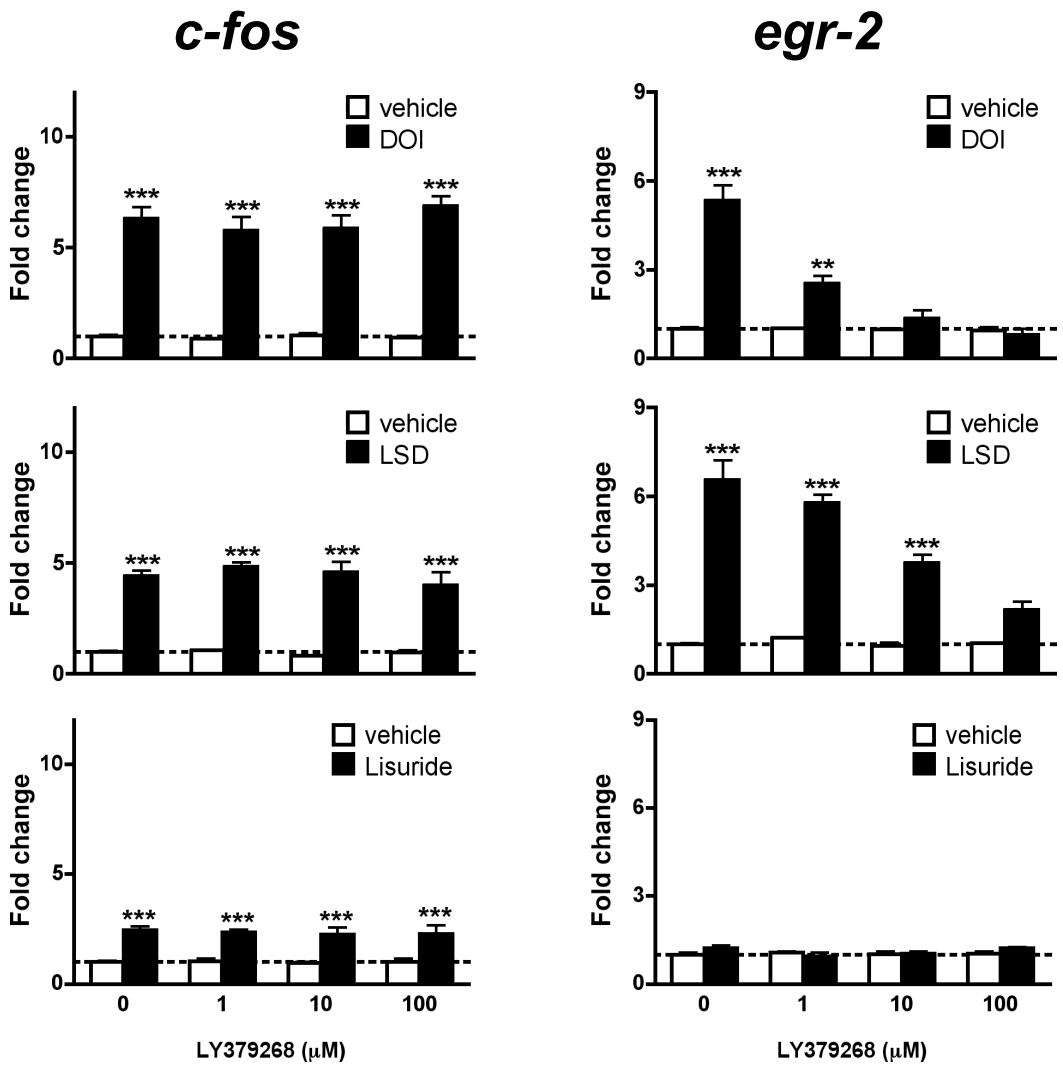

Supplementary Fig. 10

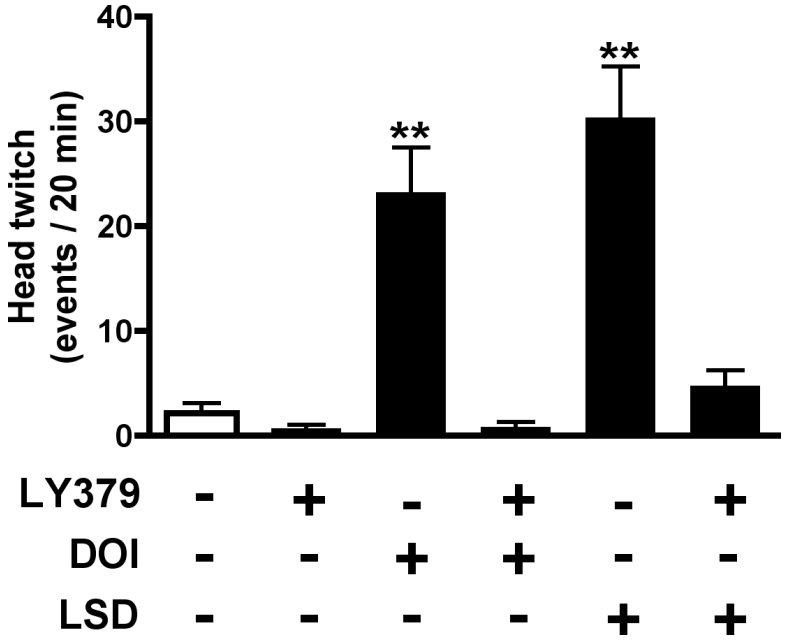

Supplementary Fig. S11

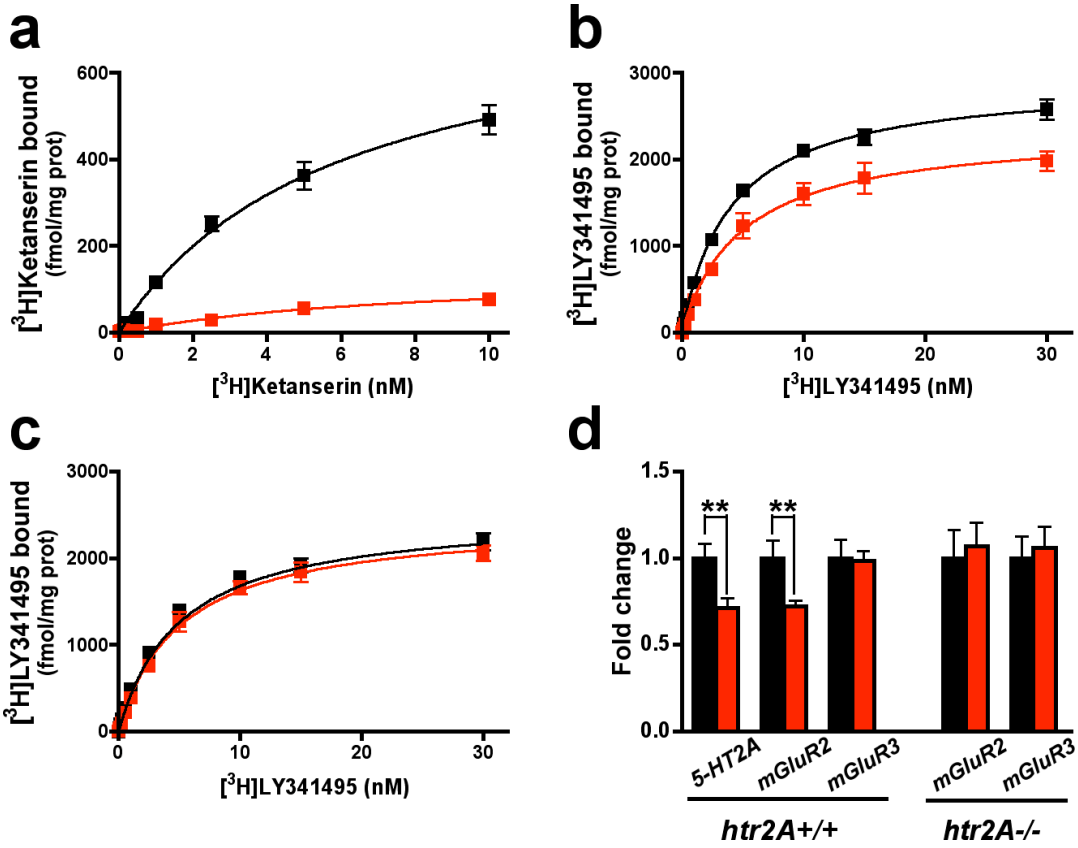

Supplementary Fig. S12

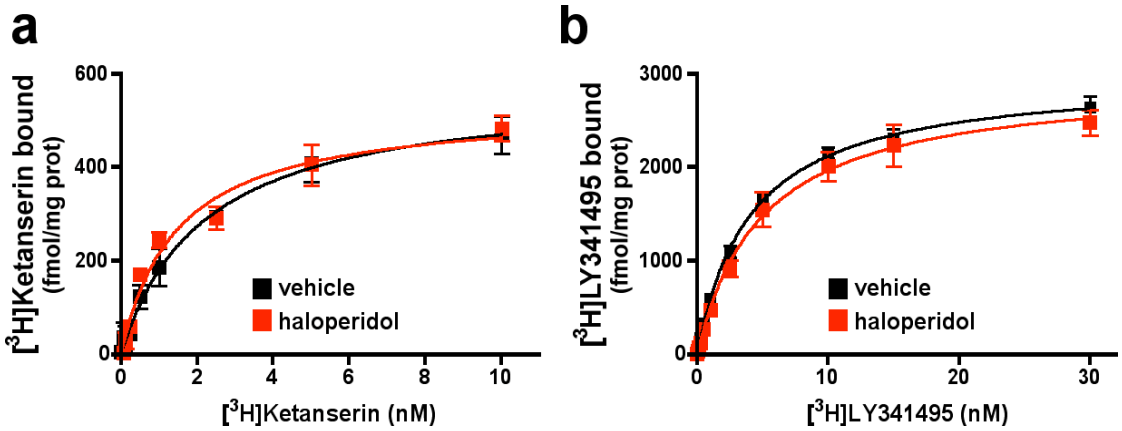

Supplementary Fig. 13

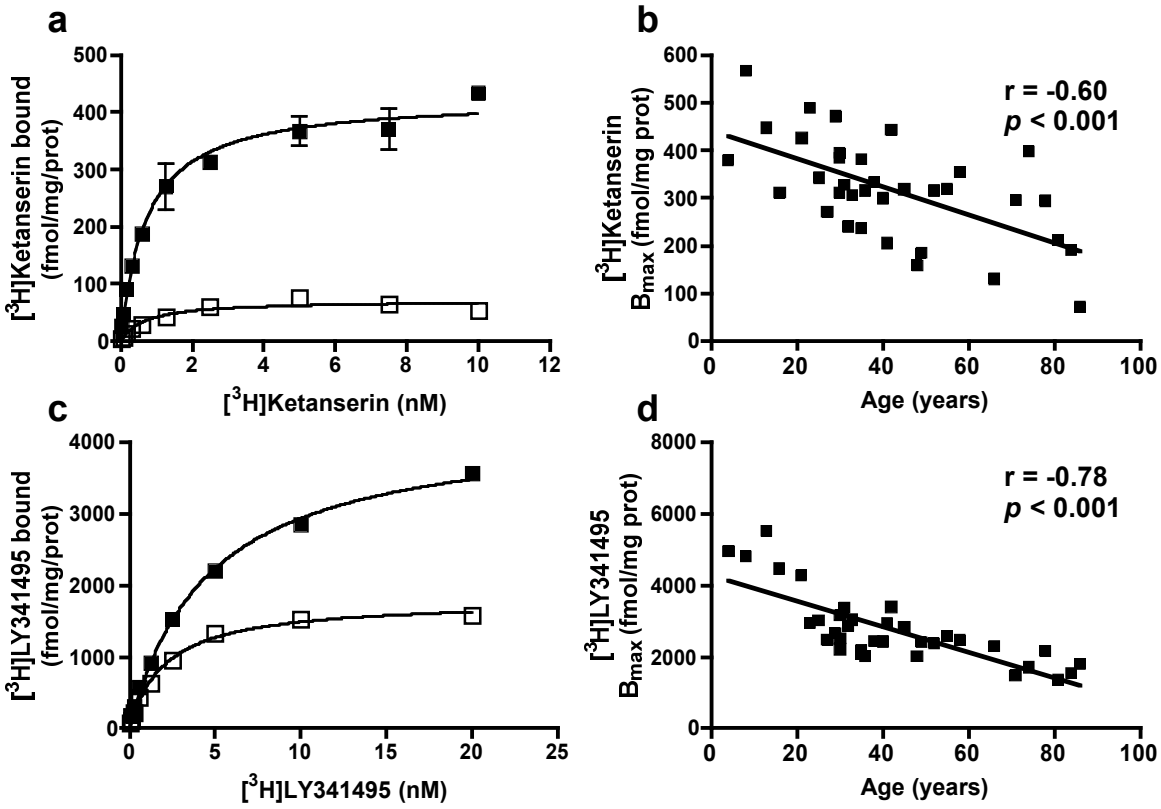

Supplementary Fig. S14